Fig. I The Nepal Himalaya and its neighbouring regions.
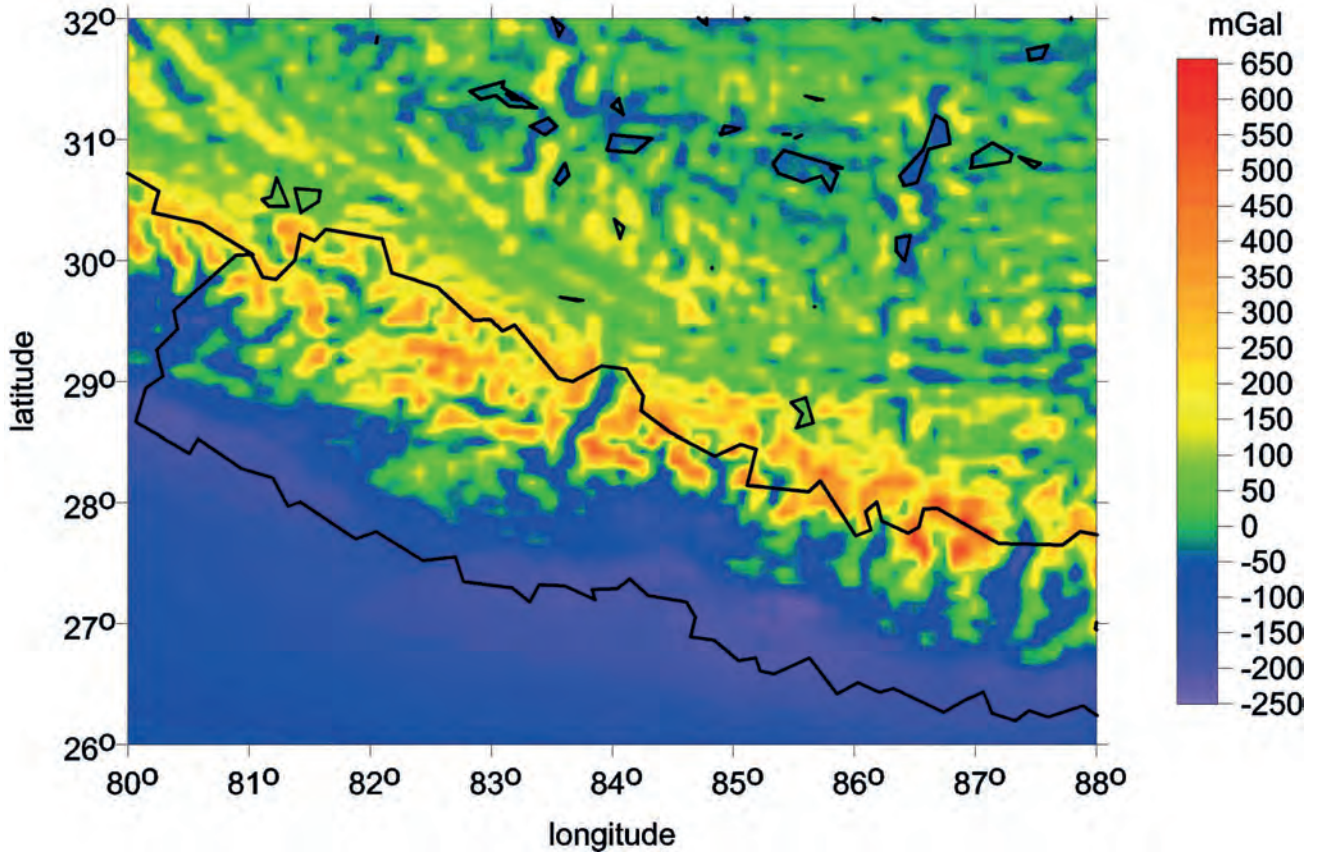

Fig. Ia The gravity anomalies Δg.
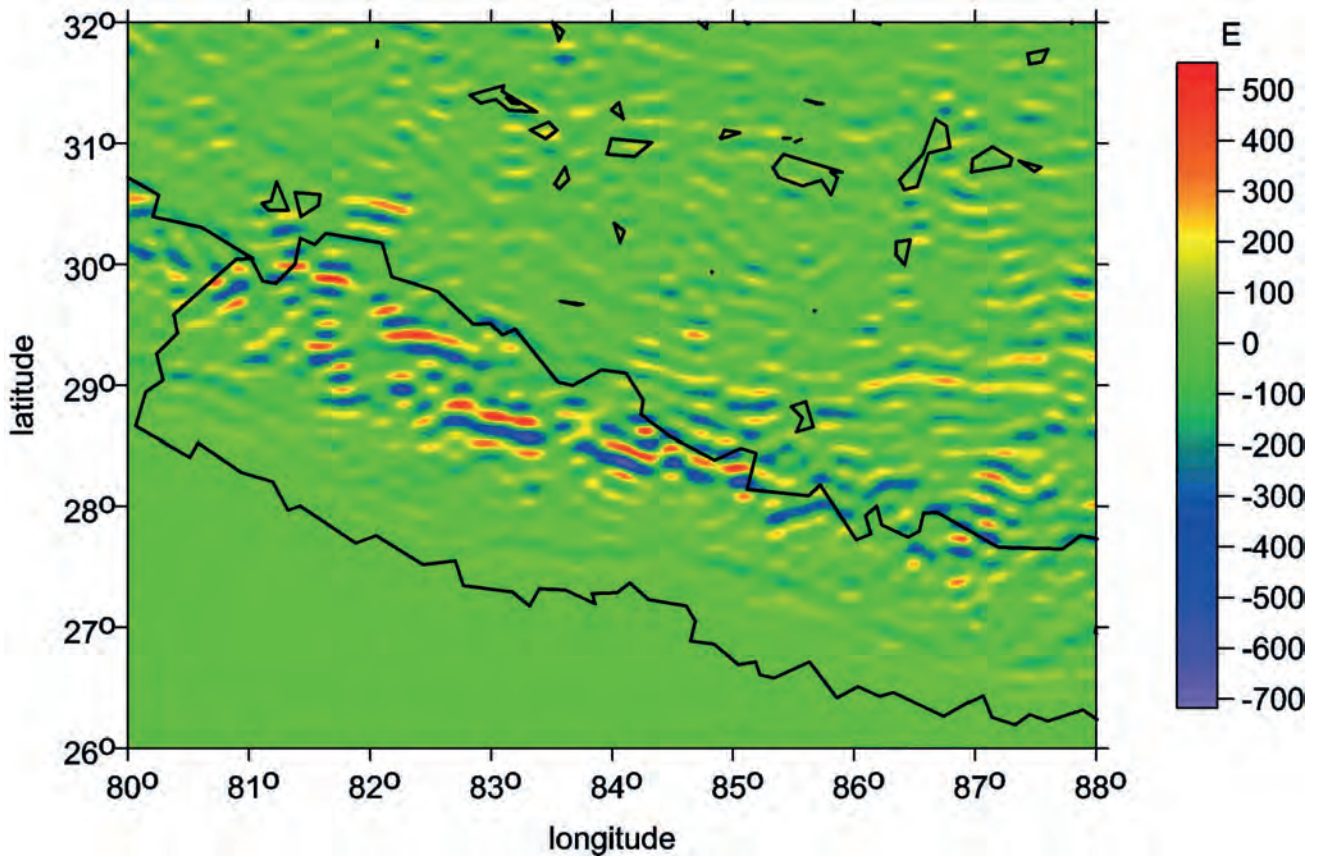

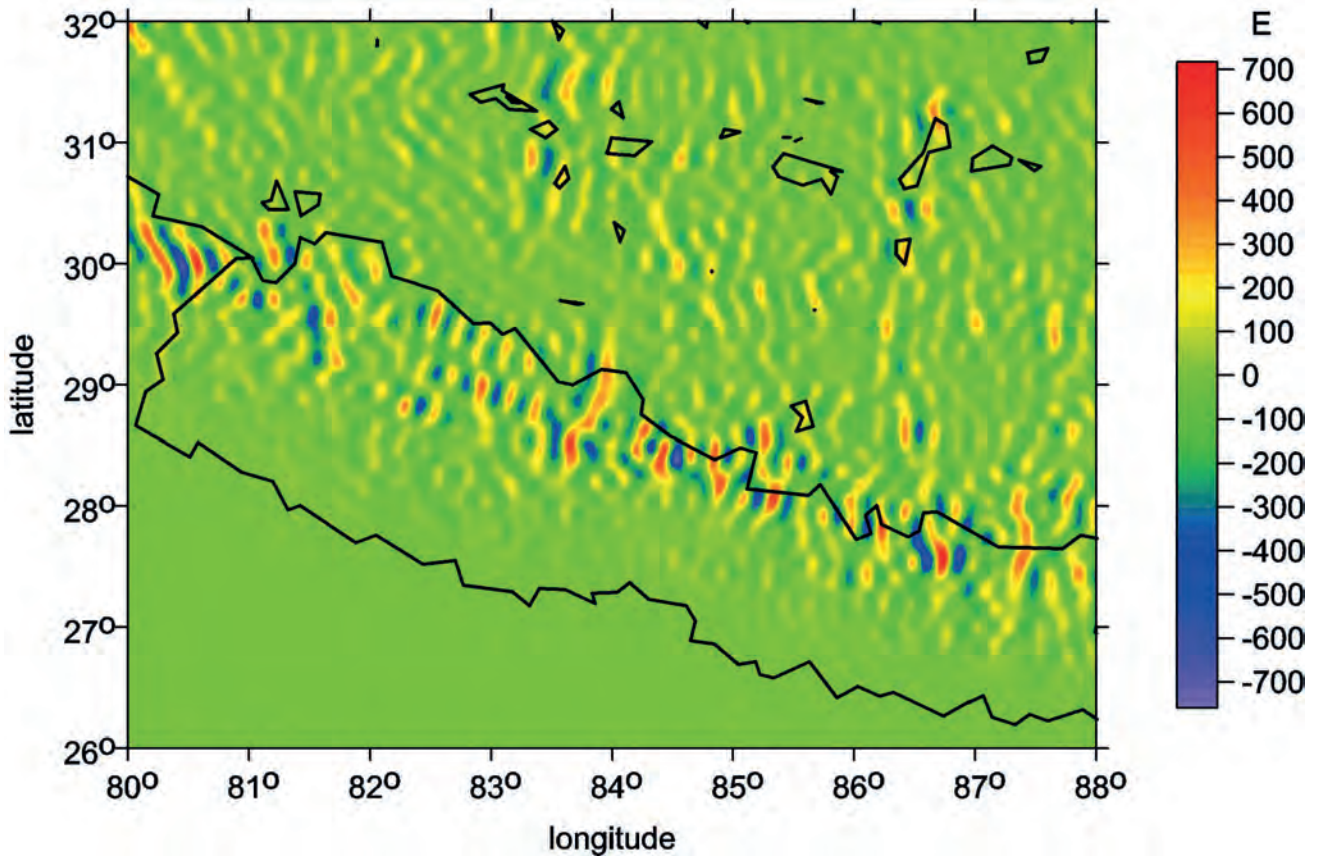**Fig. Ib** The second derivative Γ_{11} of the disturbing gravitational potential.

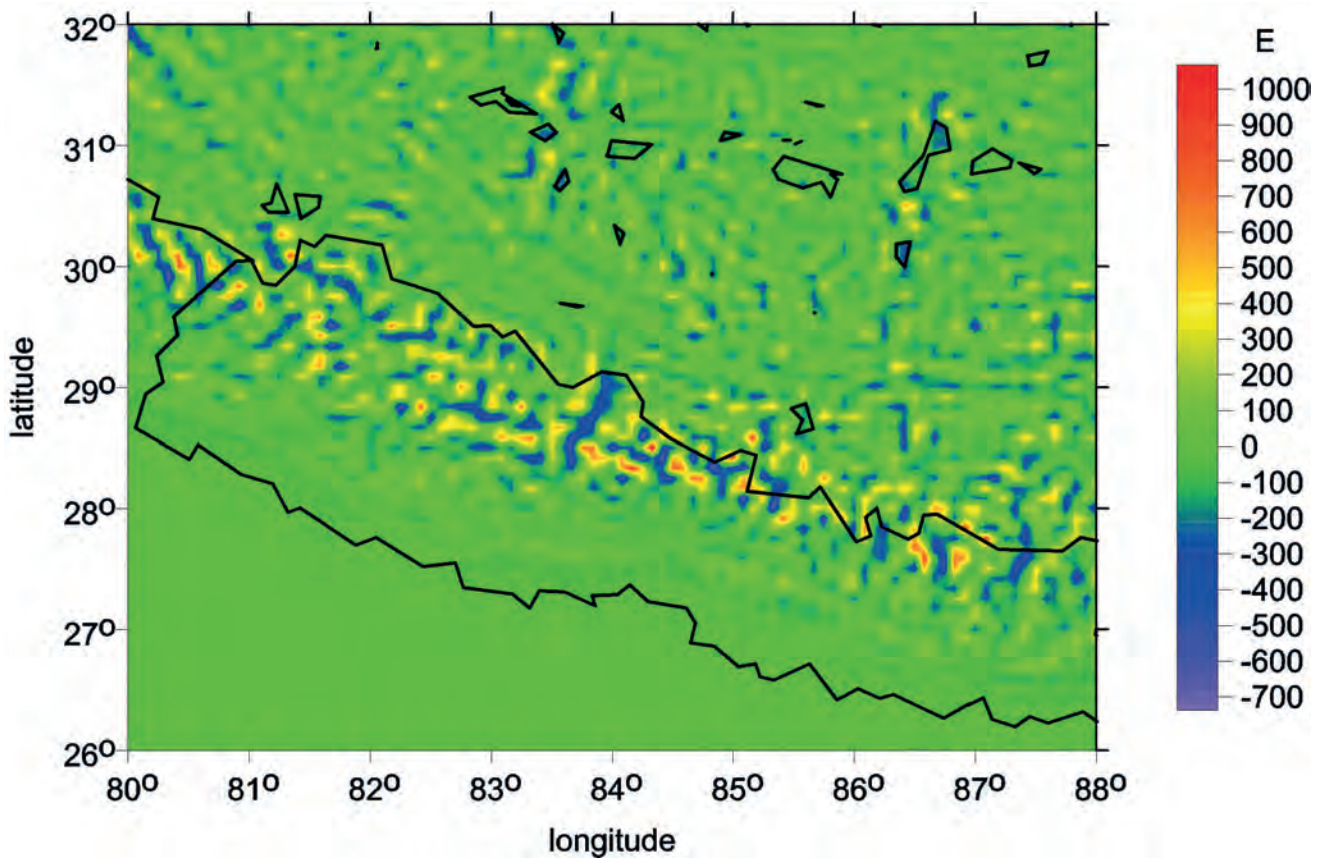**Fig. Ic** The second derivative Γ_{22} of the disturbing gravitational potential.

Fig. Id The second derivative Γ_{33} of the disturbing gravitational potential.

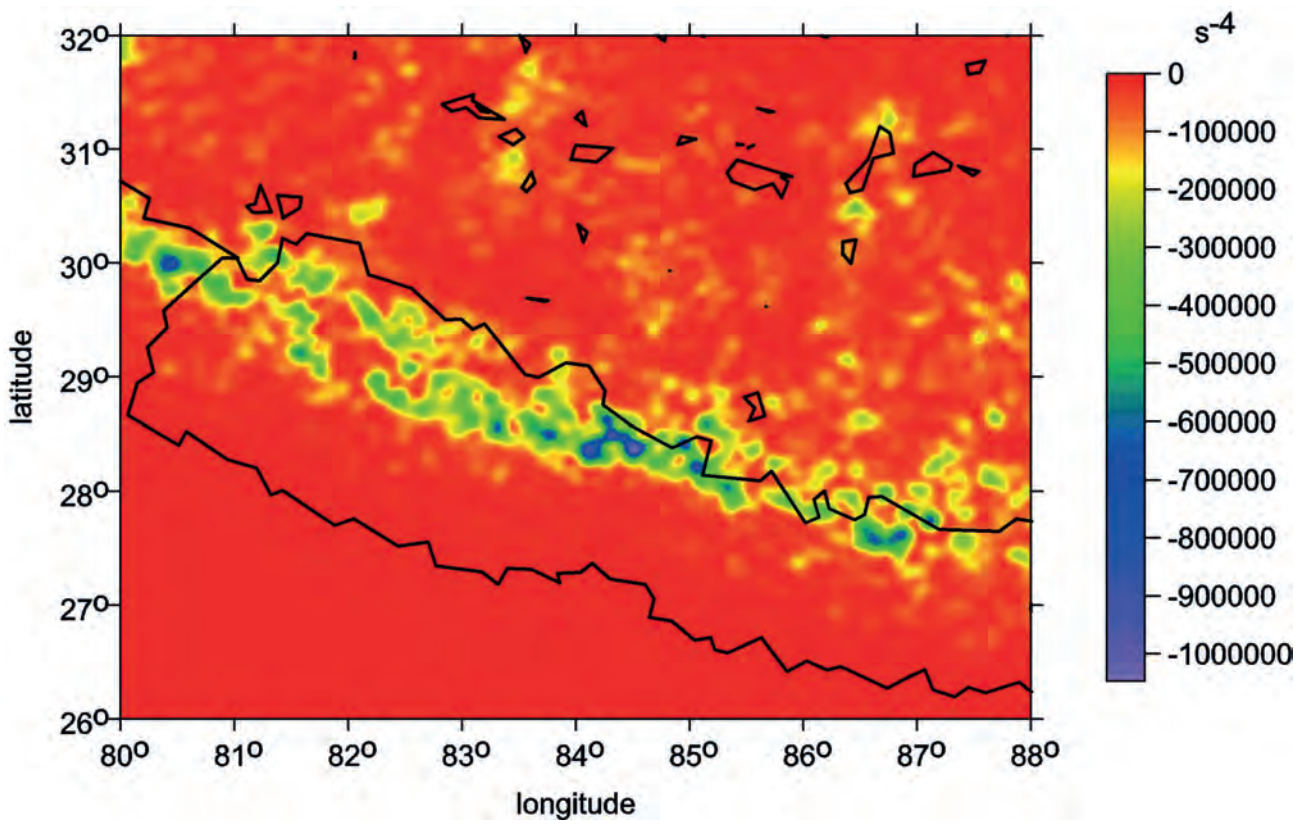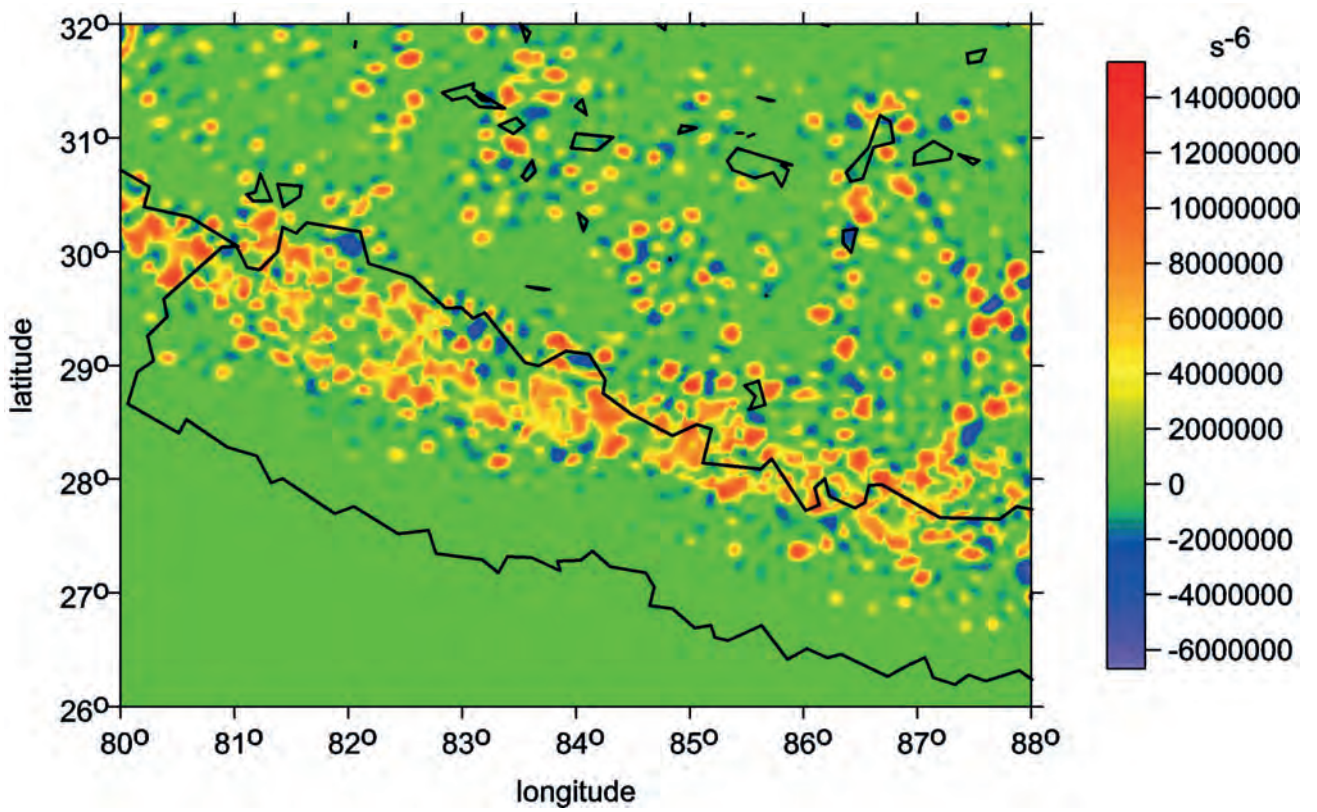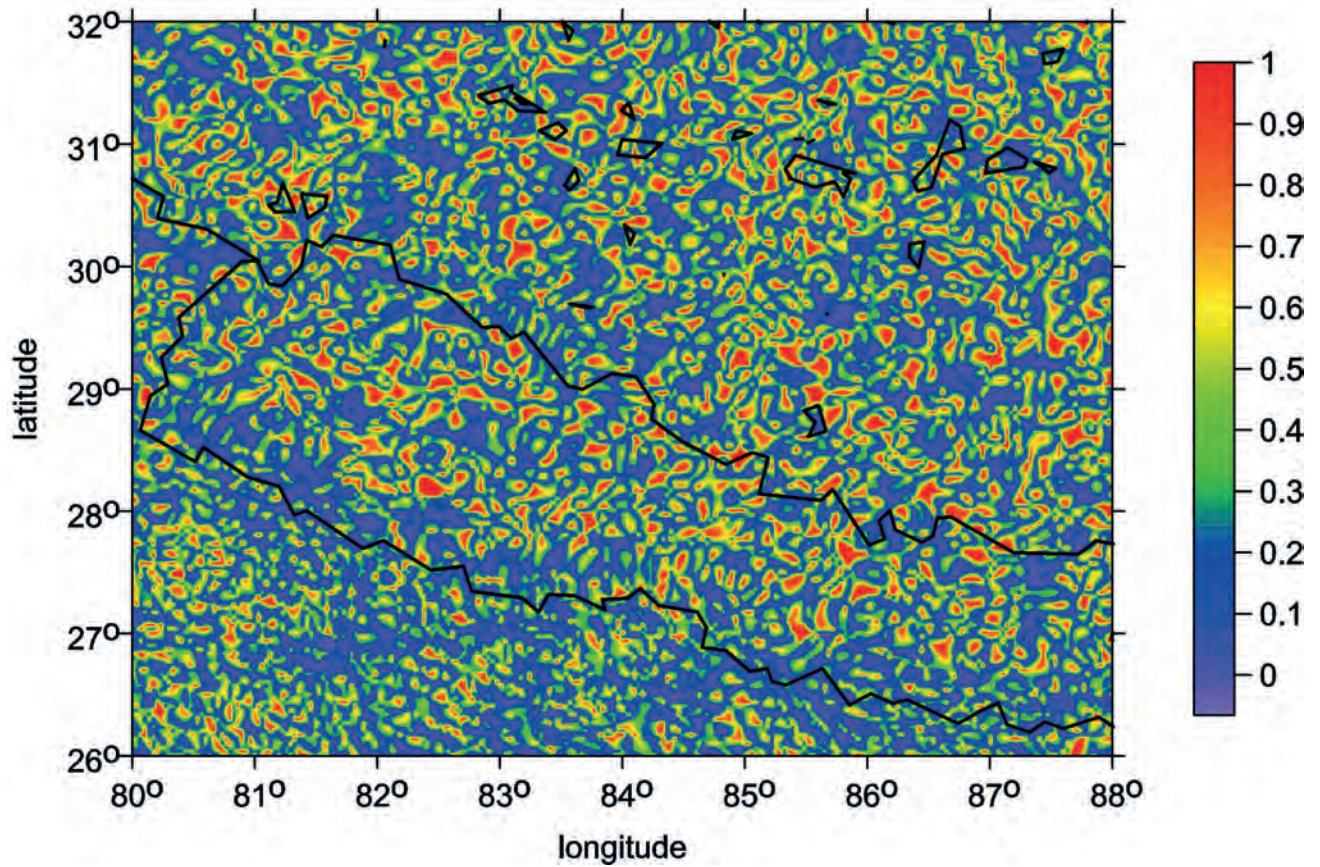**Fig. 1e** The invariant I_1.

Fig. 1f The invariant I_2.

Fig. Ig The ratio I of the invariants I_1 and I_2.
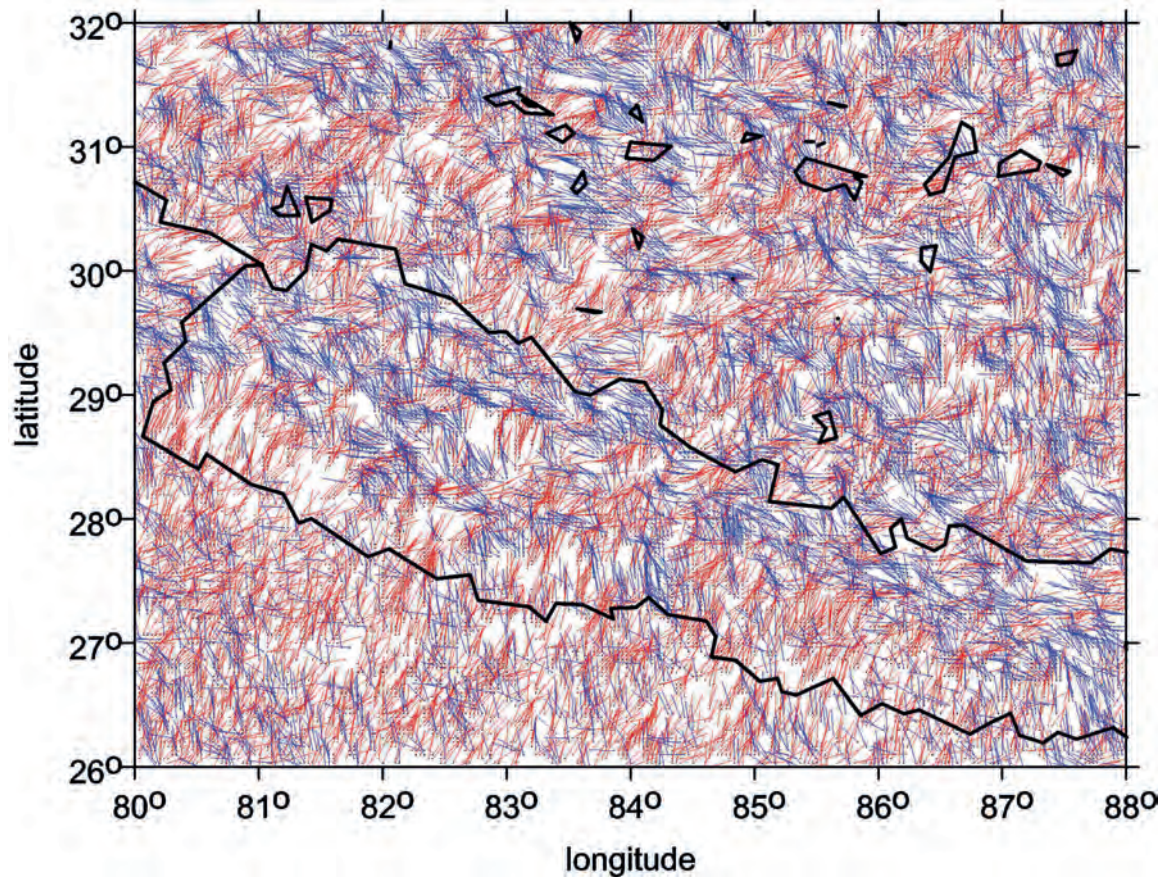

Fig. Ih The strike angle θ_S for $I > 0.3$.

Fig. Ii The strike angle θ_S for $I > 0.9$.

Fig. Ij The virtual deformations (red – dilatation, blue – compression) of the ellipse of deformation.

Fig. II The Japanese Islands in the wide collision zone of the East-Asian and West-Pacific lithospheric plates.

Fig. IIa The gravity anomalies Δg.

Fig. IIb The second derivative Γ_{33} of the disturbing gravitational potential.
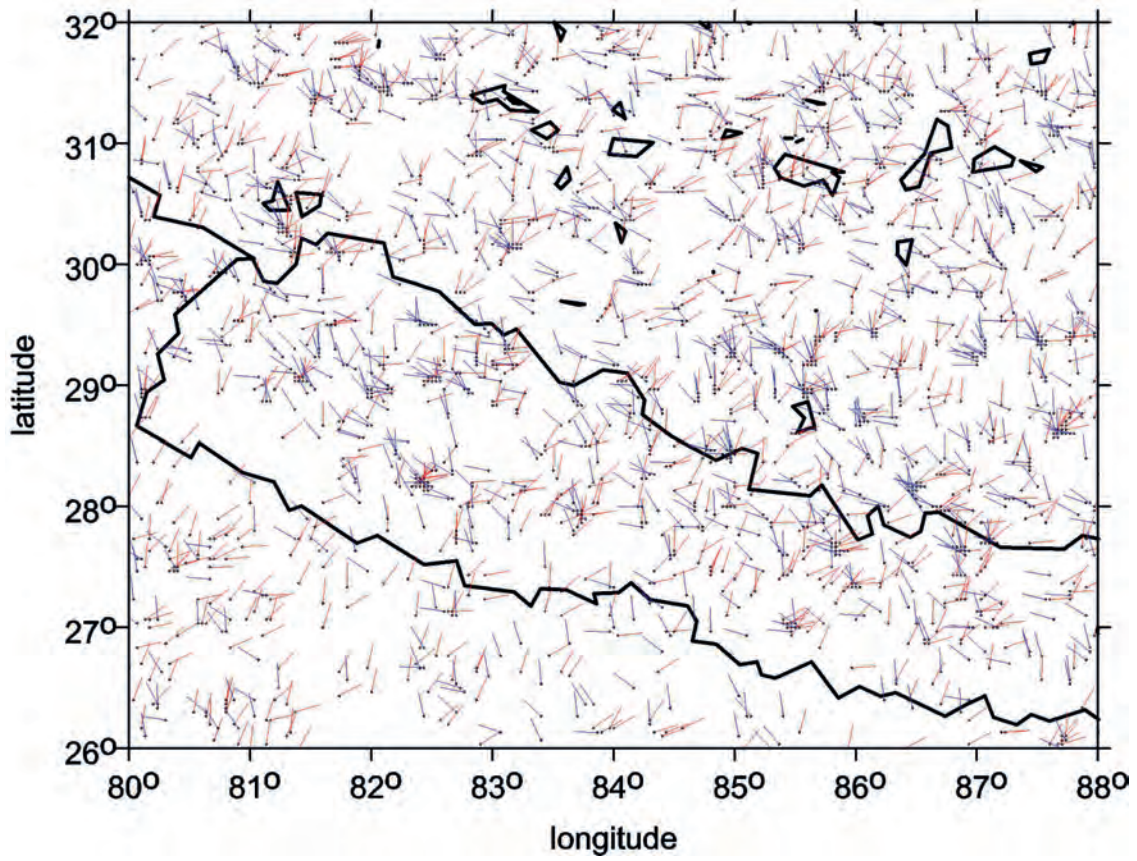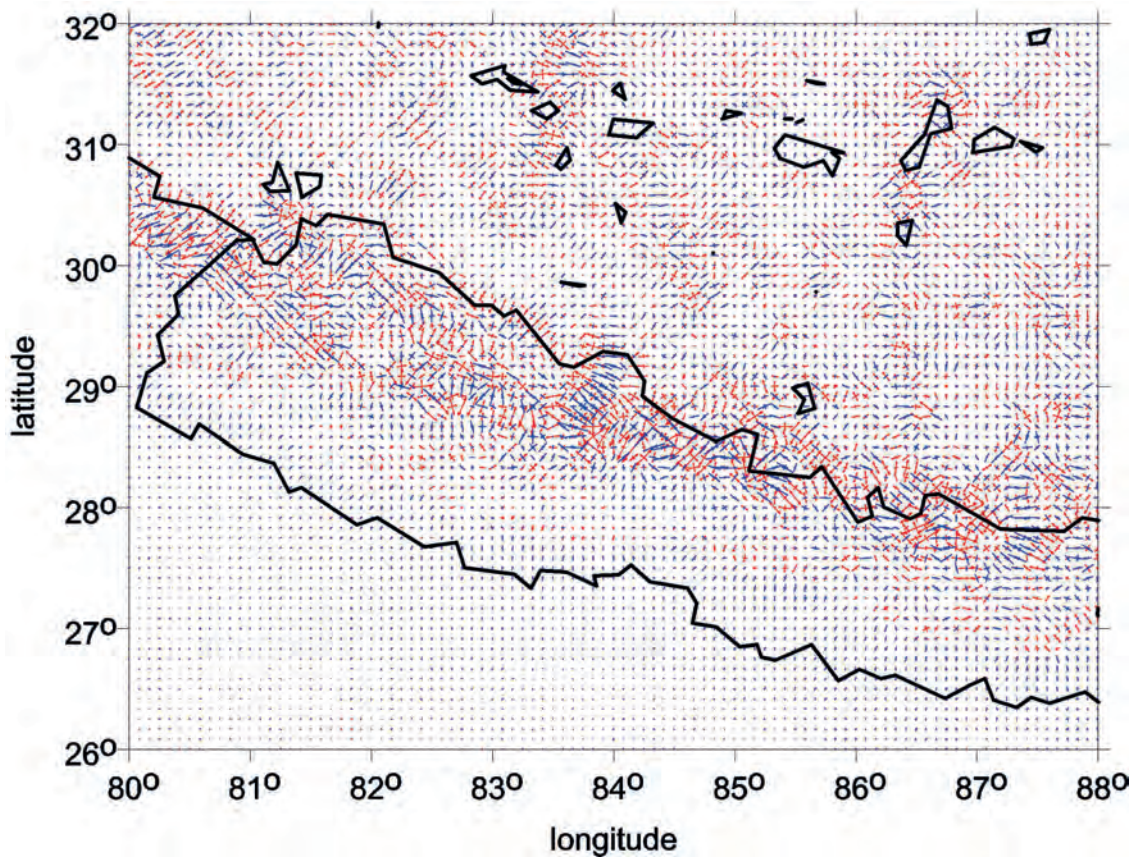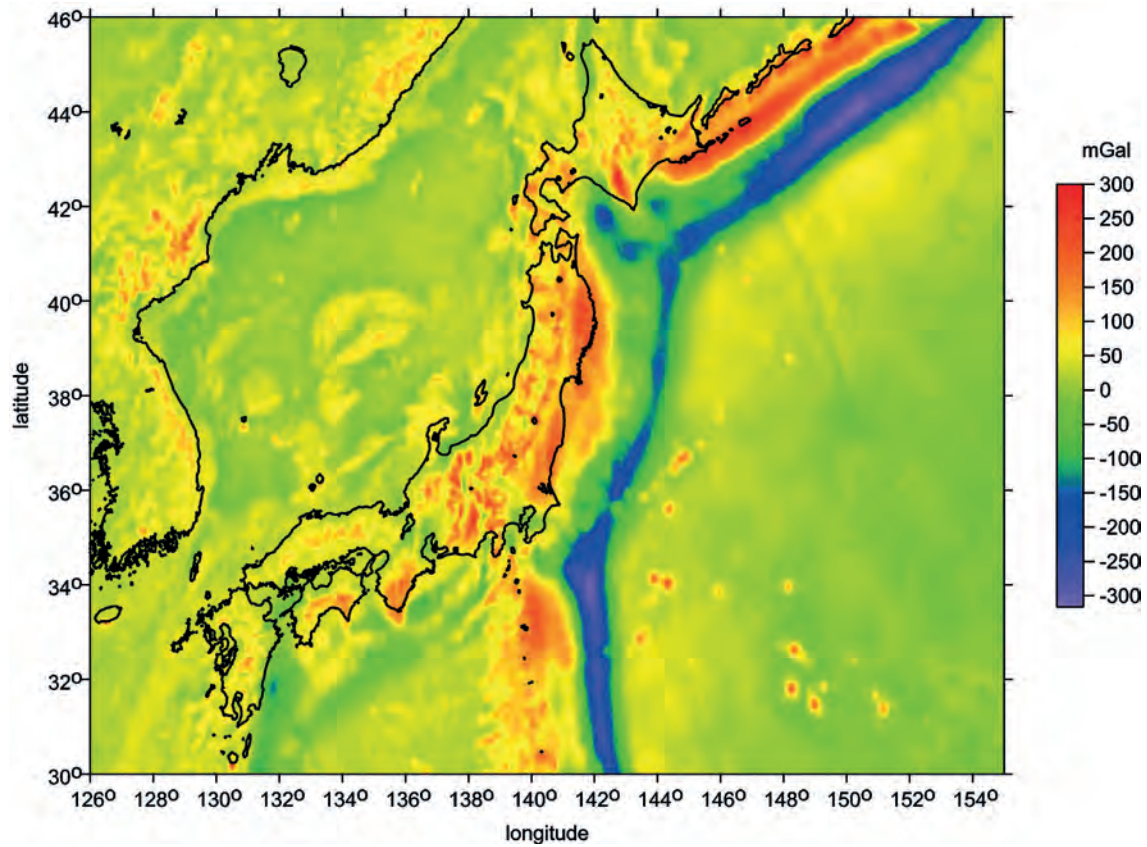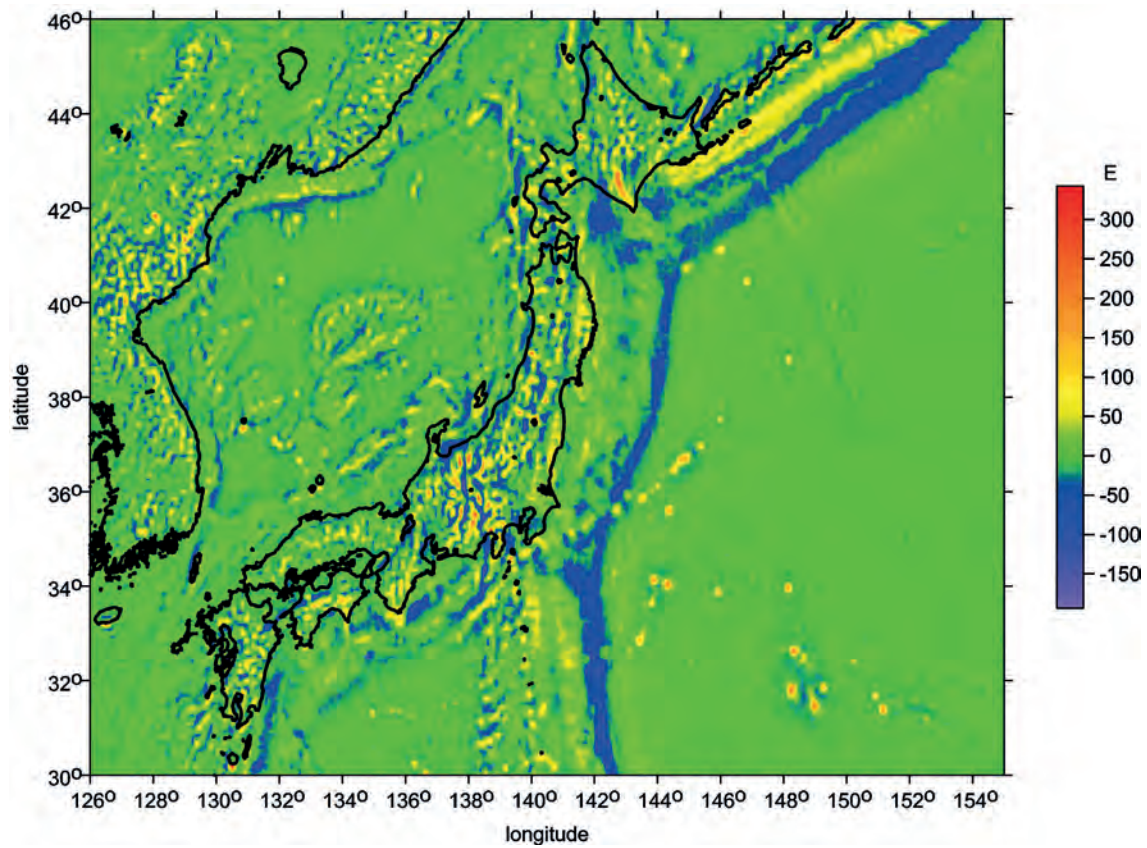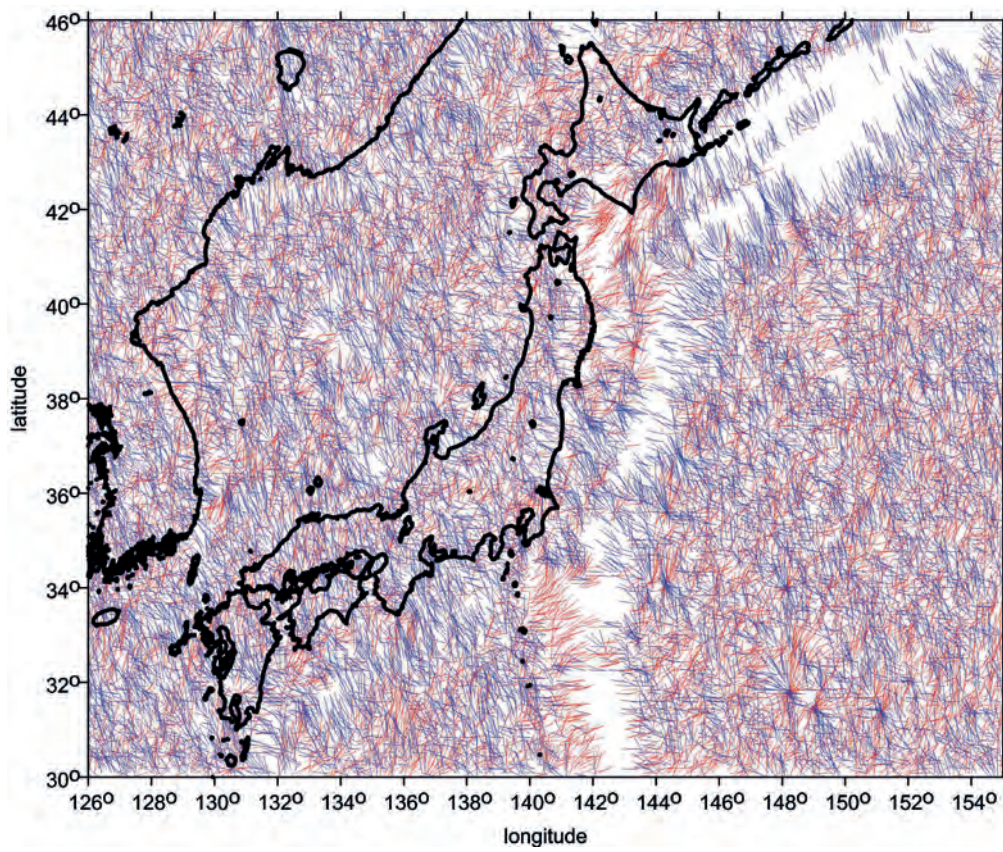
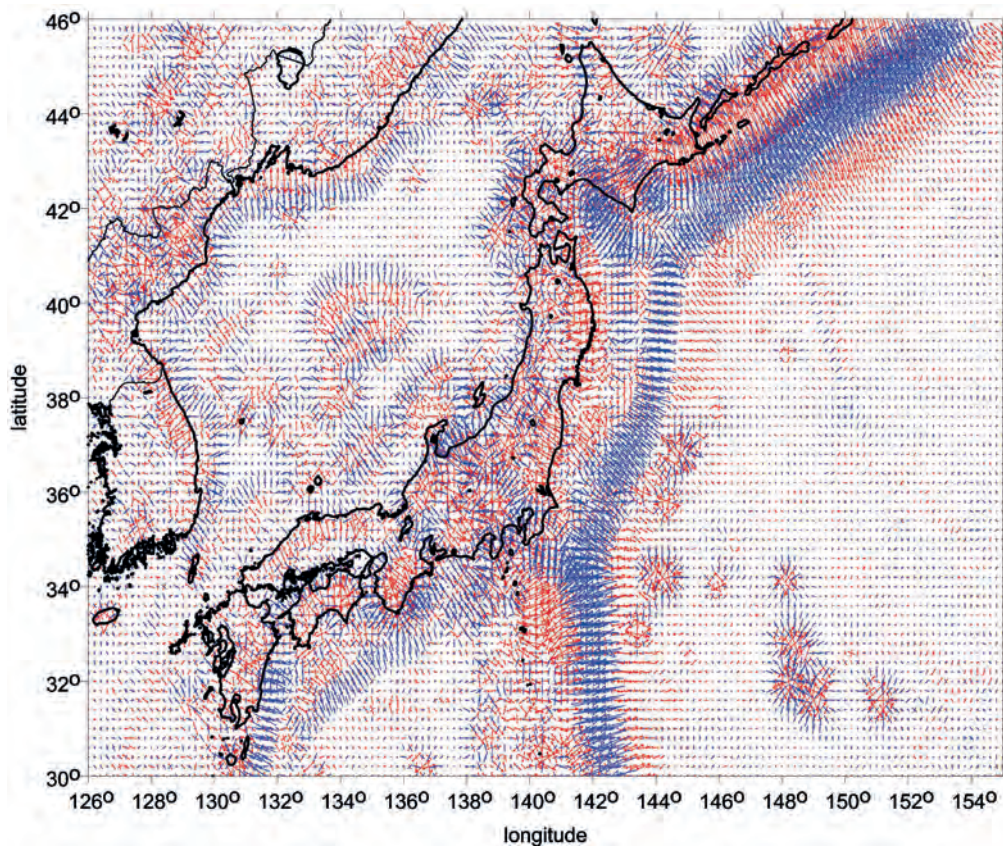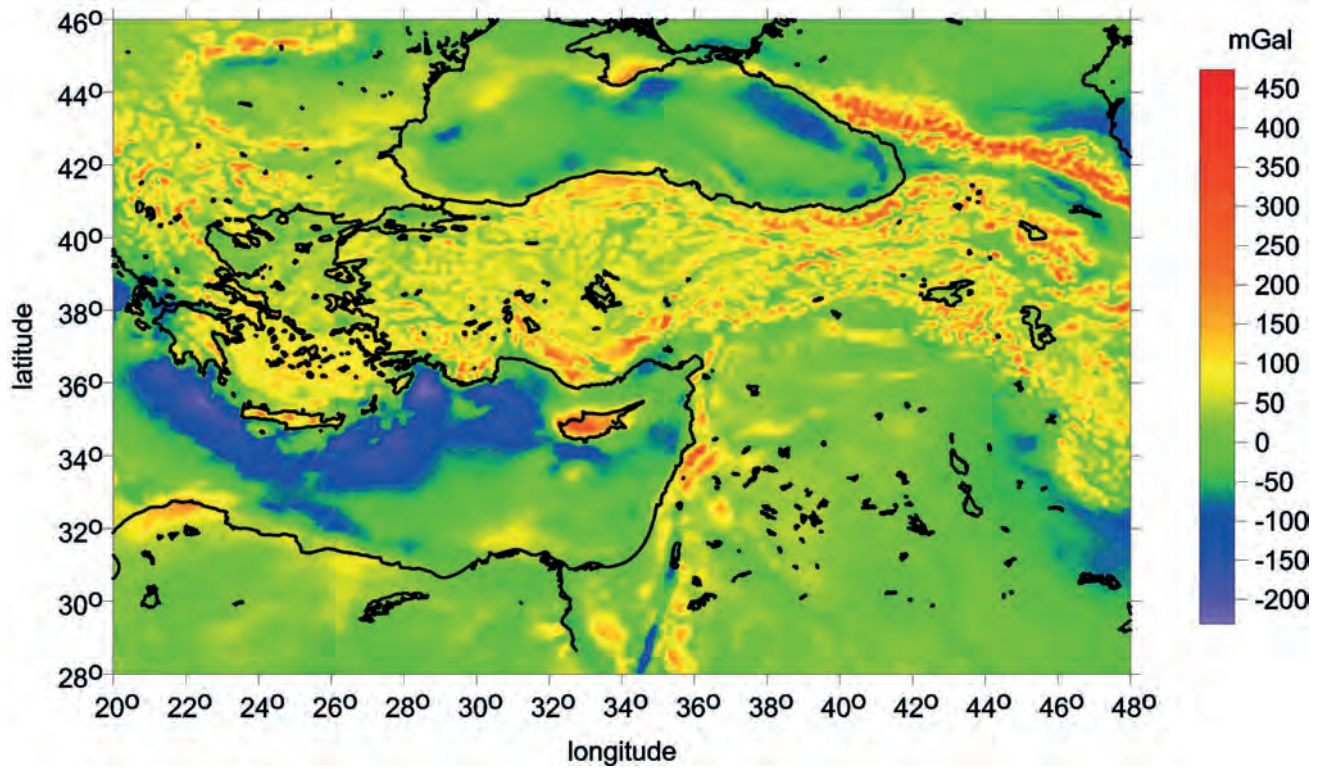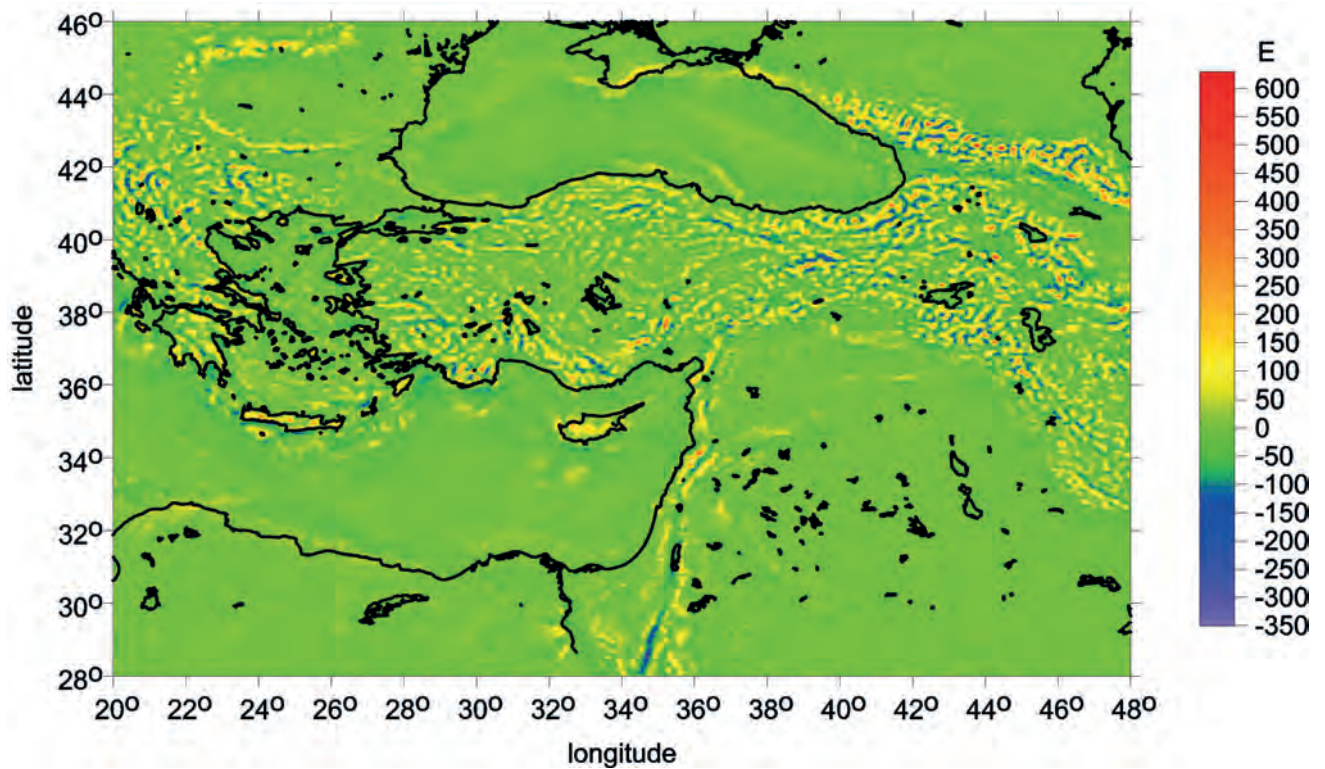**Fig. IIc** The strike angle θ_S for $I > 0.3$.

Fig. IId The virtual deformations (red – dilatation, blue – compression) of the ellipse of deformation.

Fig. III The broad contact region of north-eastern Africa, south-western Asia and south-eastern Europe.

Fig. IIIa The gravity anomalies Δ*g*.

Fig. IIIb The second derivative Γ_{33} of the disturbing gravitational potential.
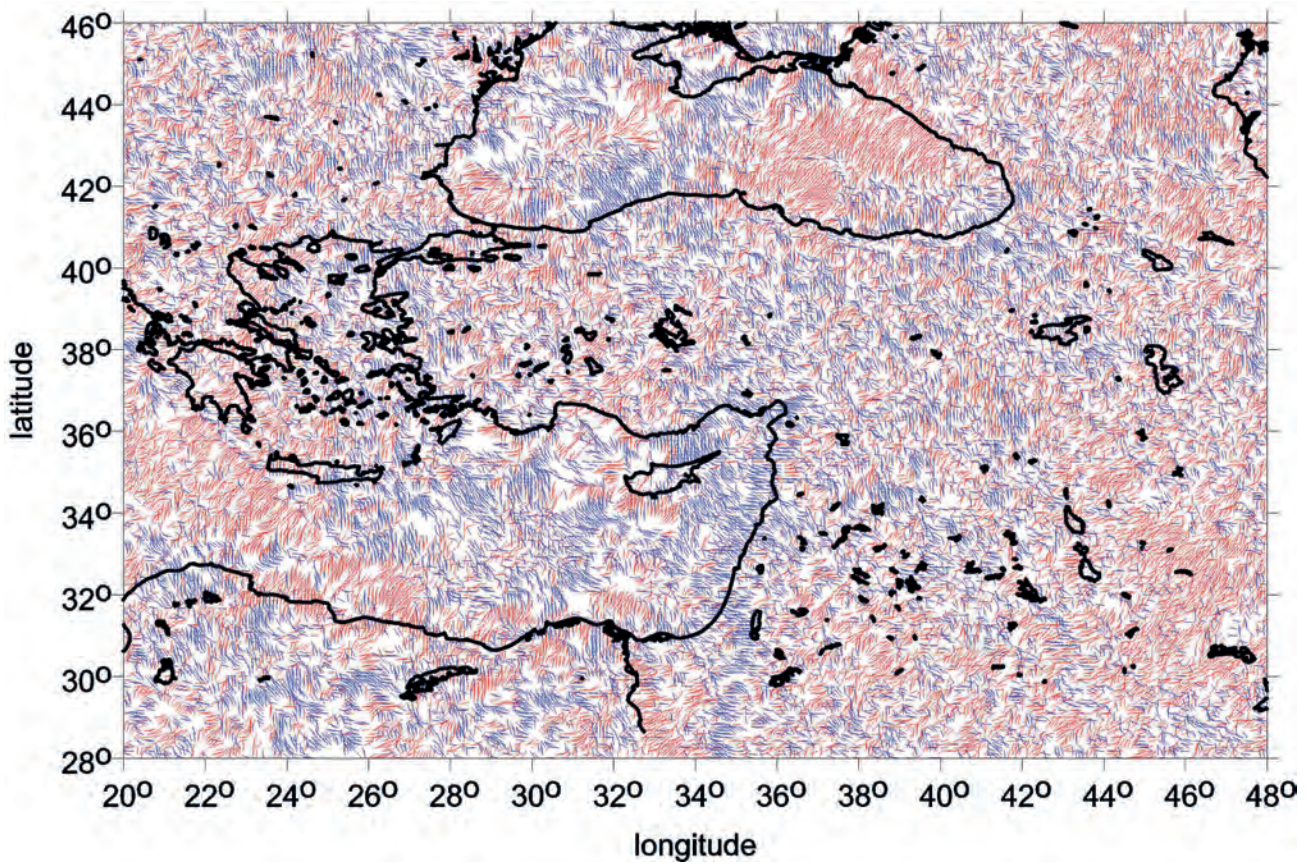
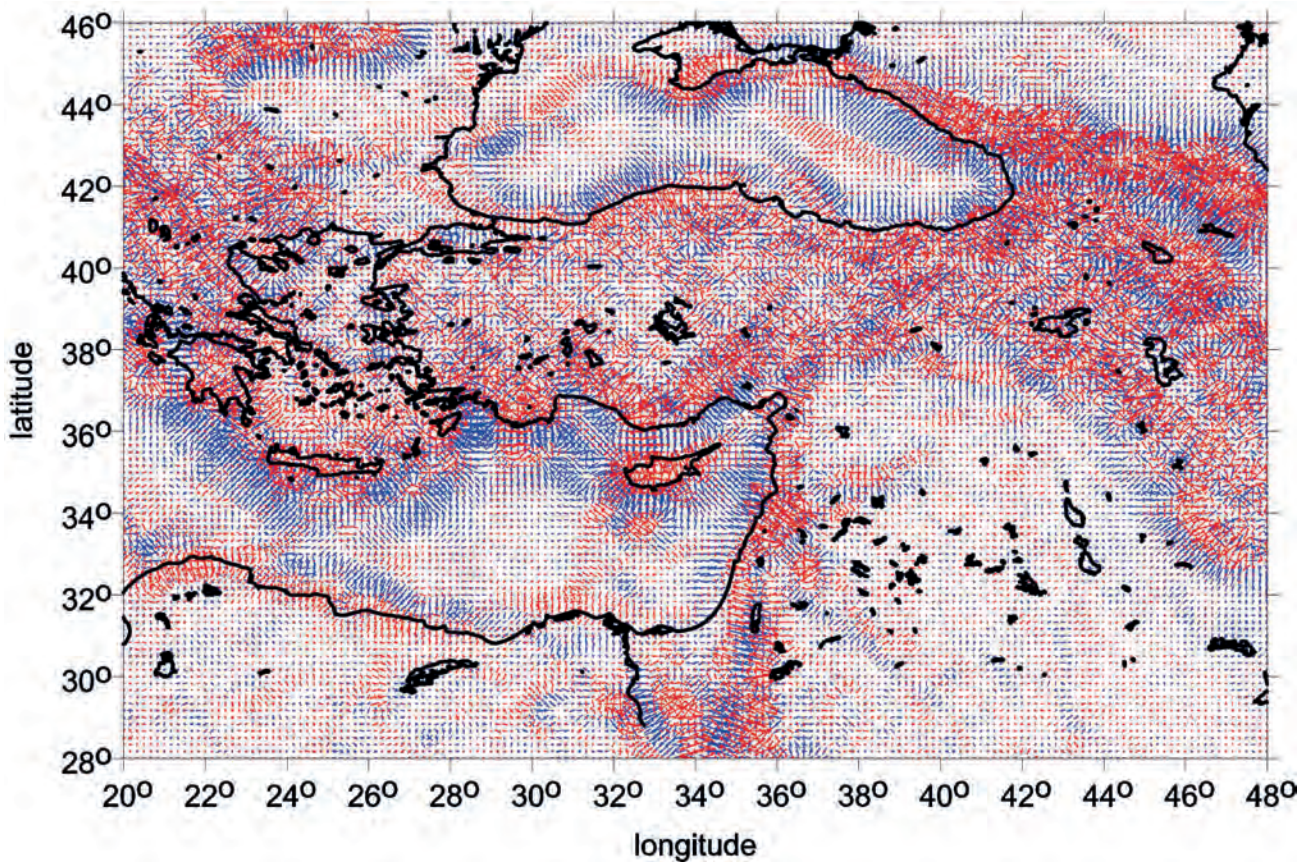**Fig. IIIc** The strike angle θ_S for $I > 0.3$.

Fig. IIId The virtual deformations (red – dilatation, blue – compression) of the ellipse of deformation.

Fig. IV Central Europe with conspicuous contacts between the three extensive orogenetic units: the Eastern Alps, the Bohemian Massif and the Western Carpathians.
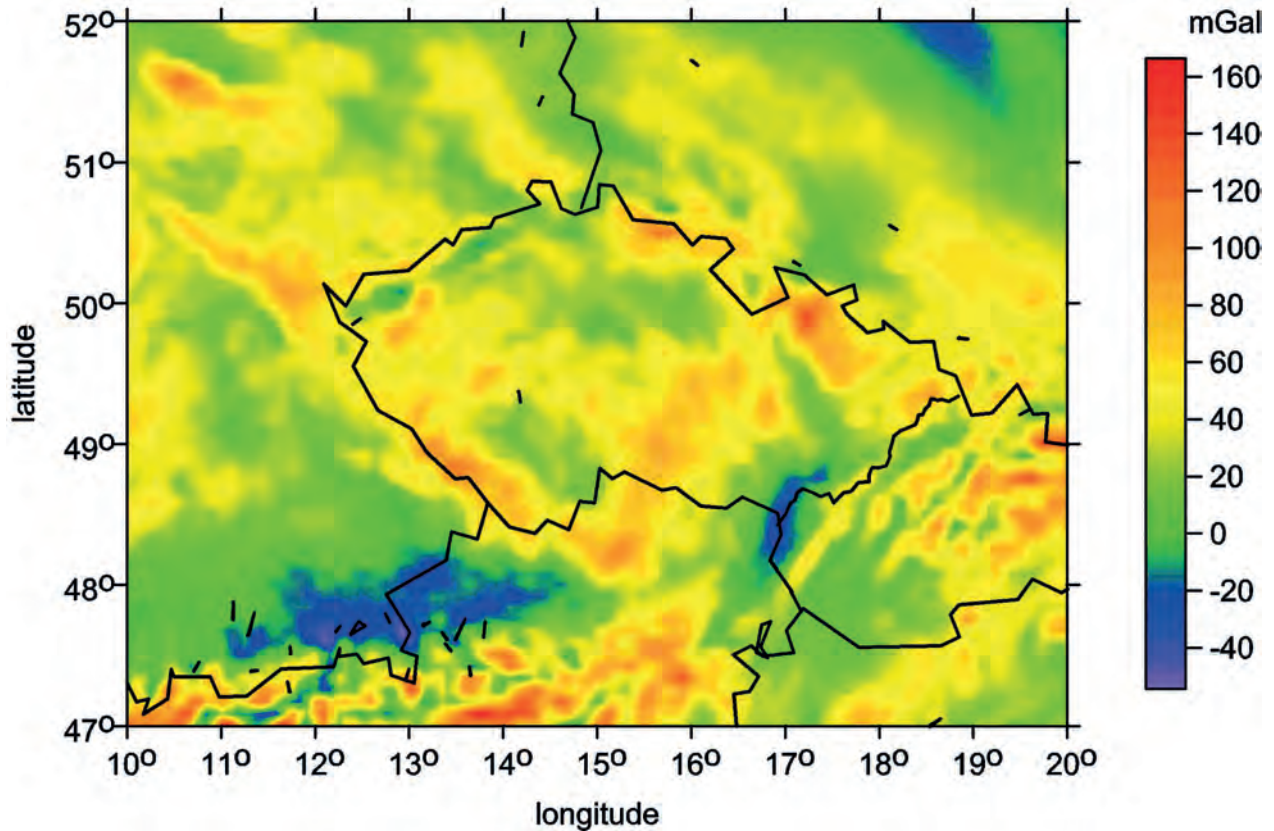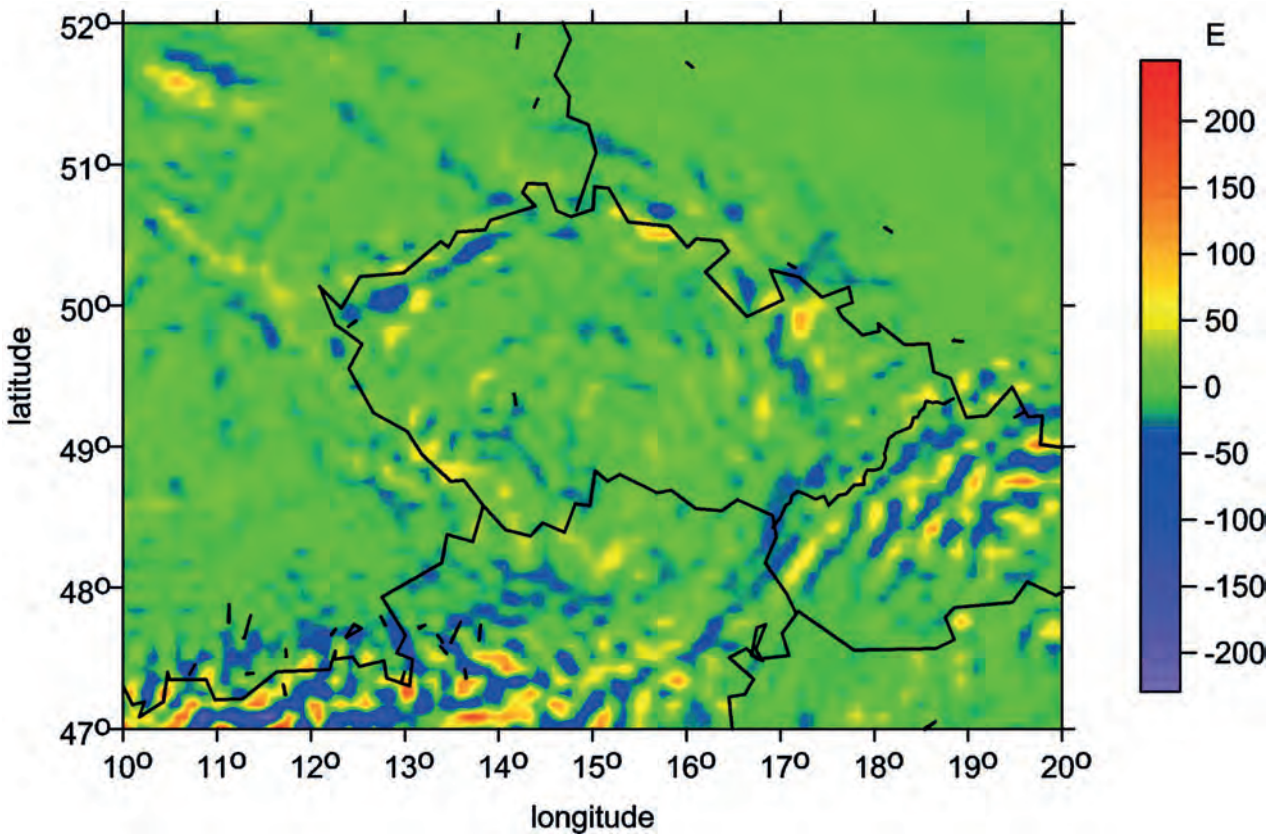

Fig. IVa The gravity anomalies Δ*g*.

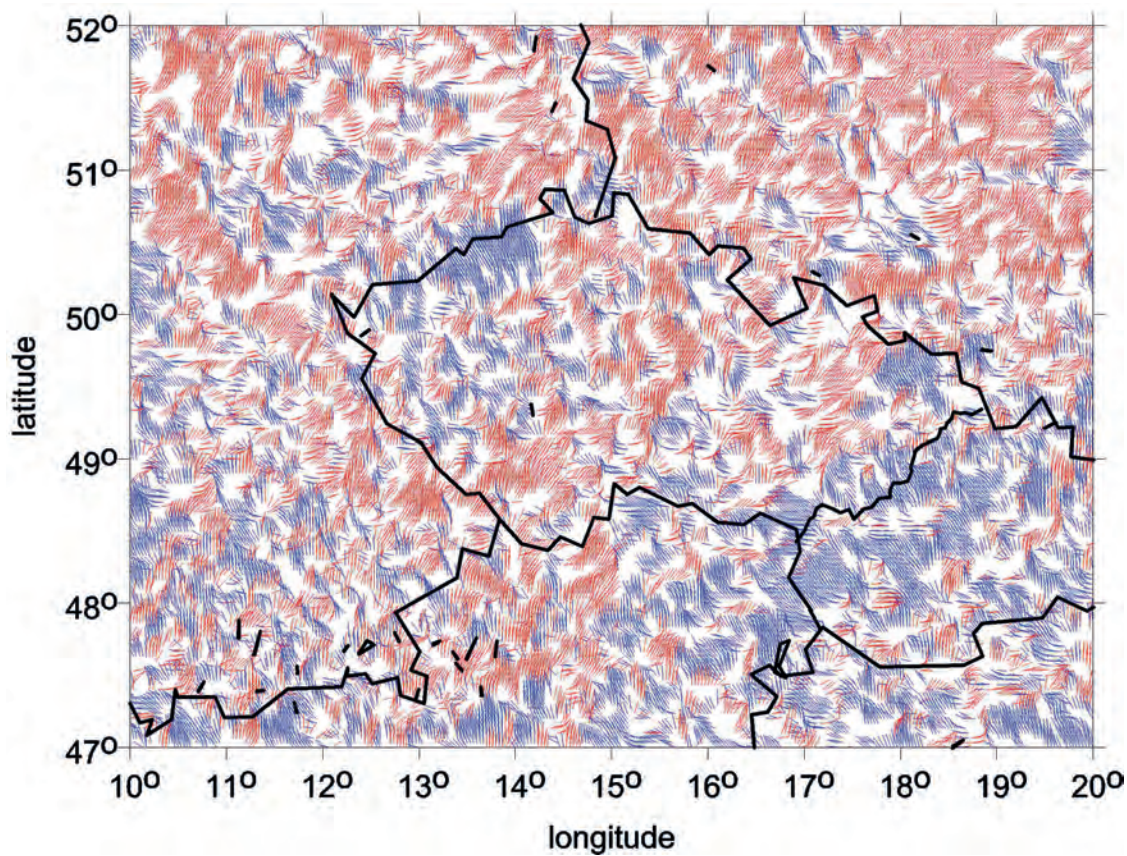**Fig. IVb** The second derivative Γ_{33} of the disturbing gravitational potential.

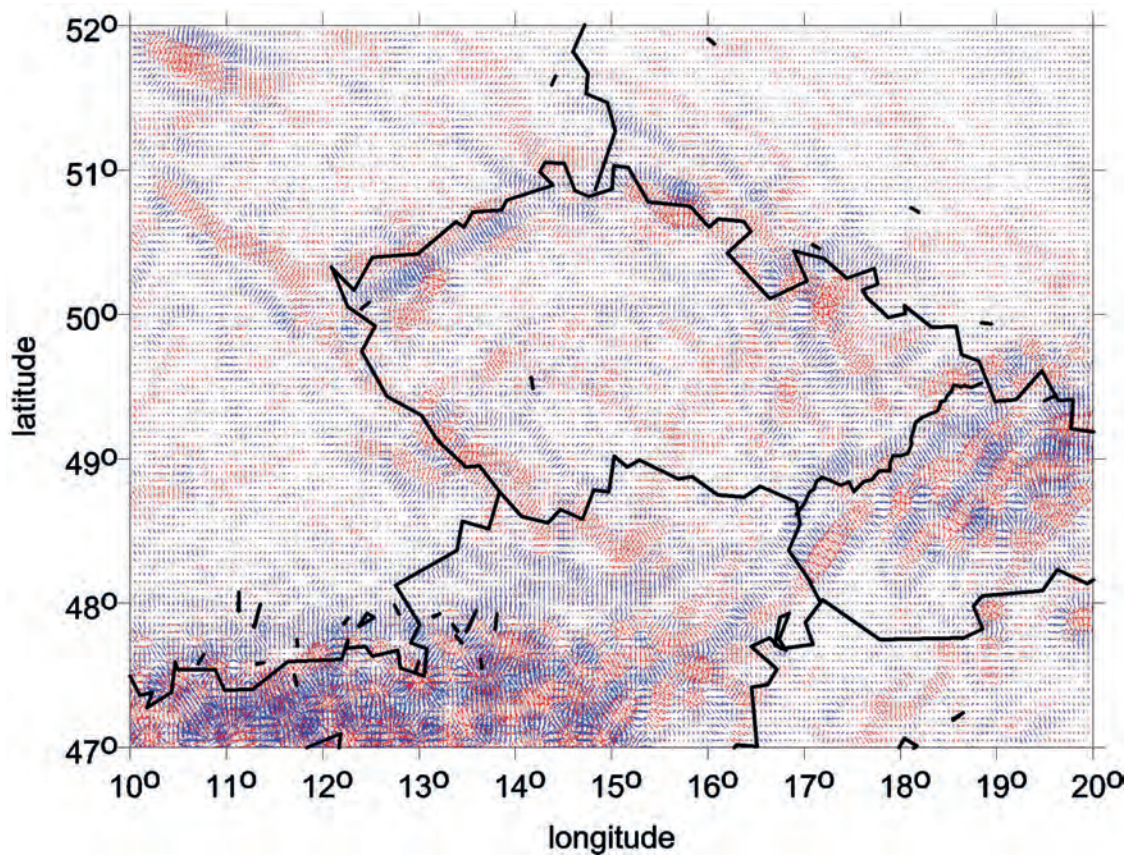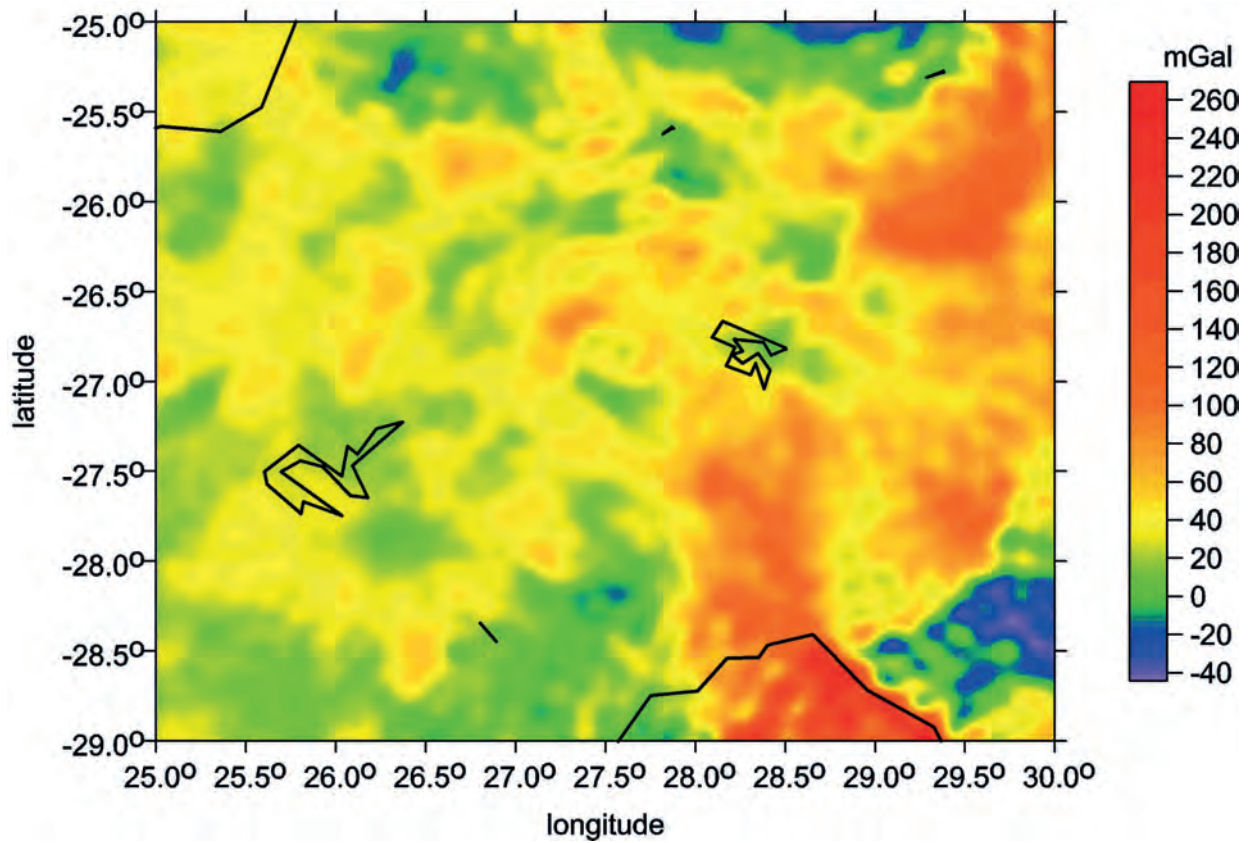**Fig. IVc** The strike angle θ_S for $I < 0.3$ (looking for flat objects).
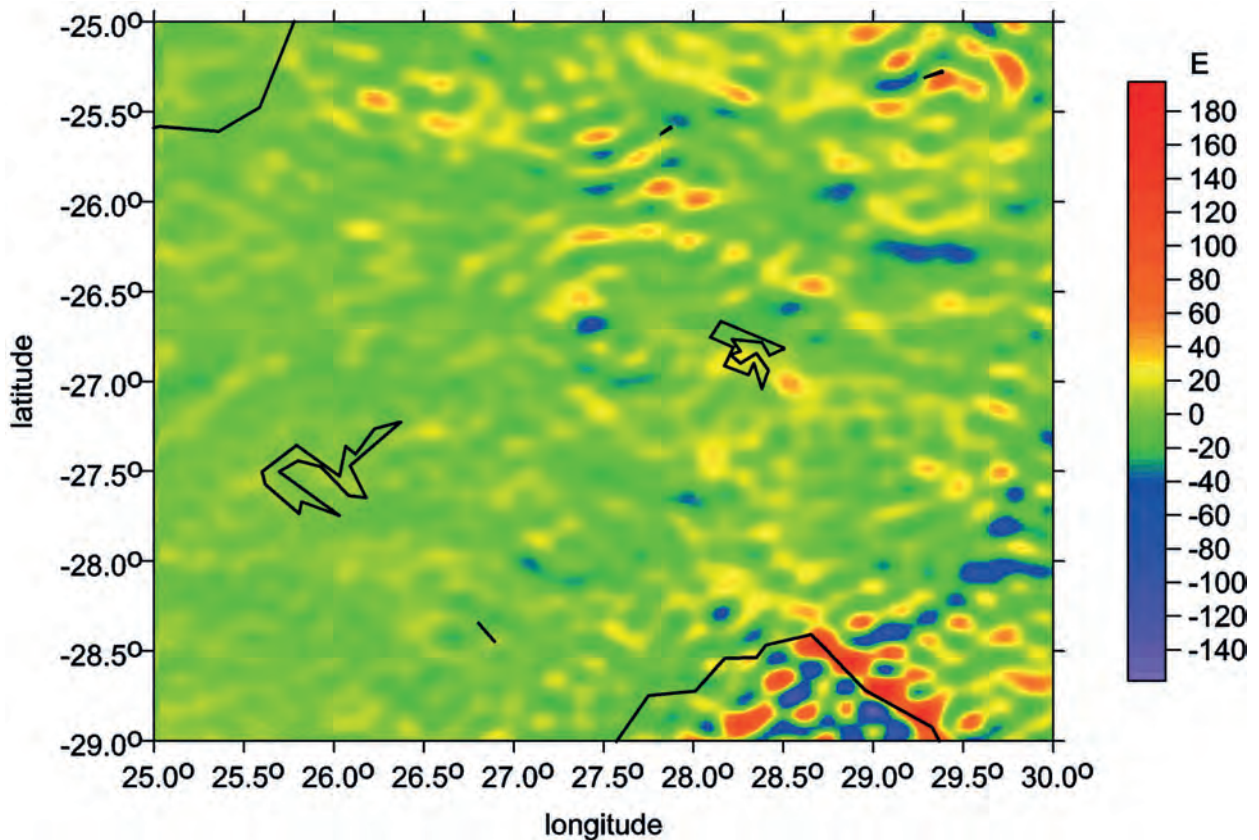

Fig. IVd The virtual deformations (red – dilatation, blue – compression) of the ellipse of deformation.

Fig. V The Vredefort impact crater in South Africa.

Fig. Va The gravity anomalies Δ*g*.

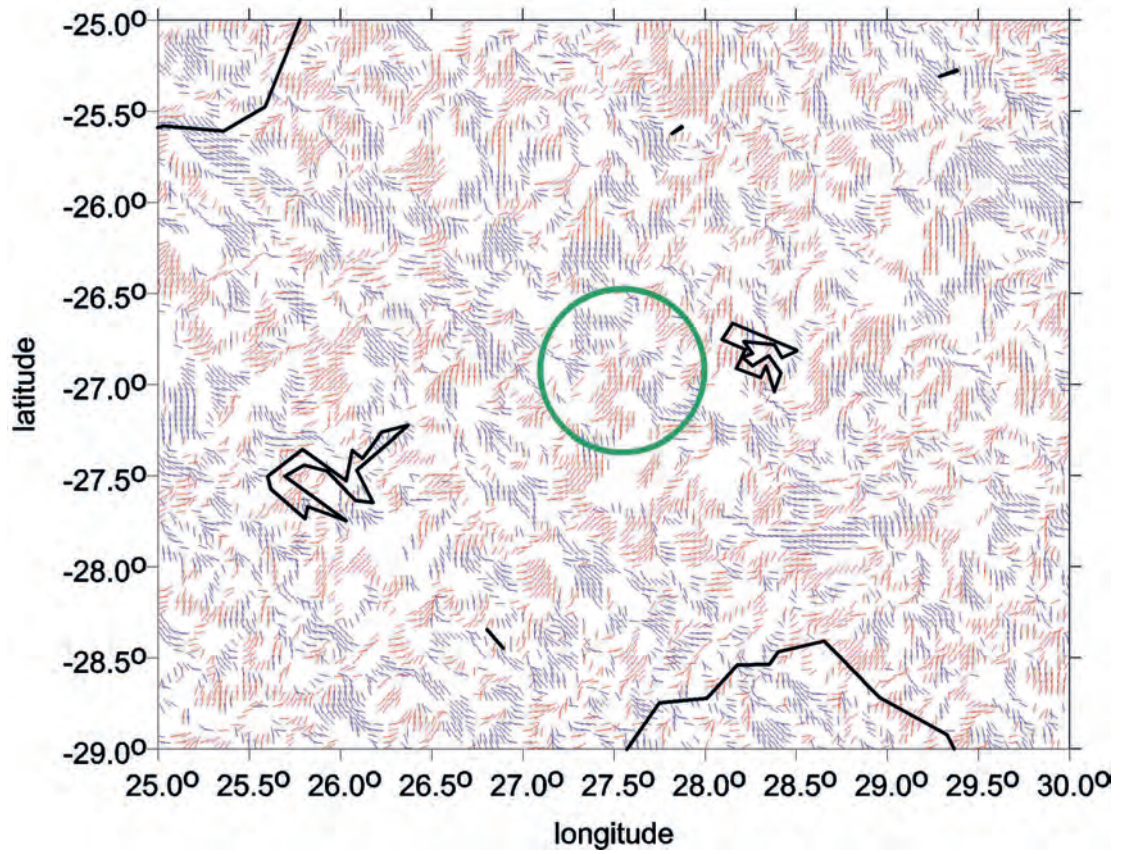**Fig. Vb** The second derivative Γ_{33} of the disturbing gravitational potential.

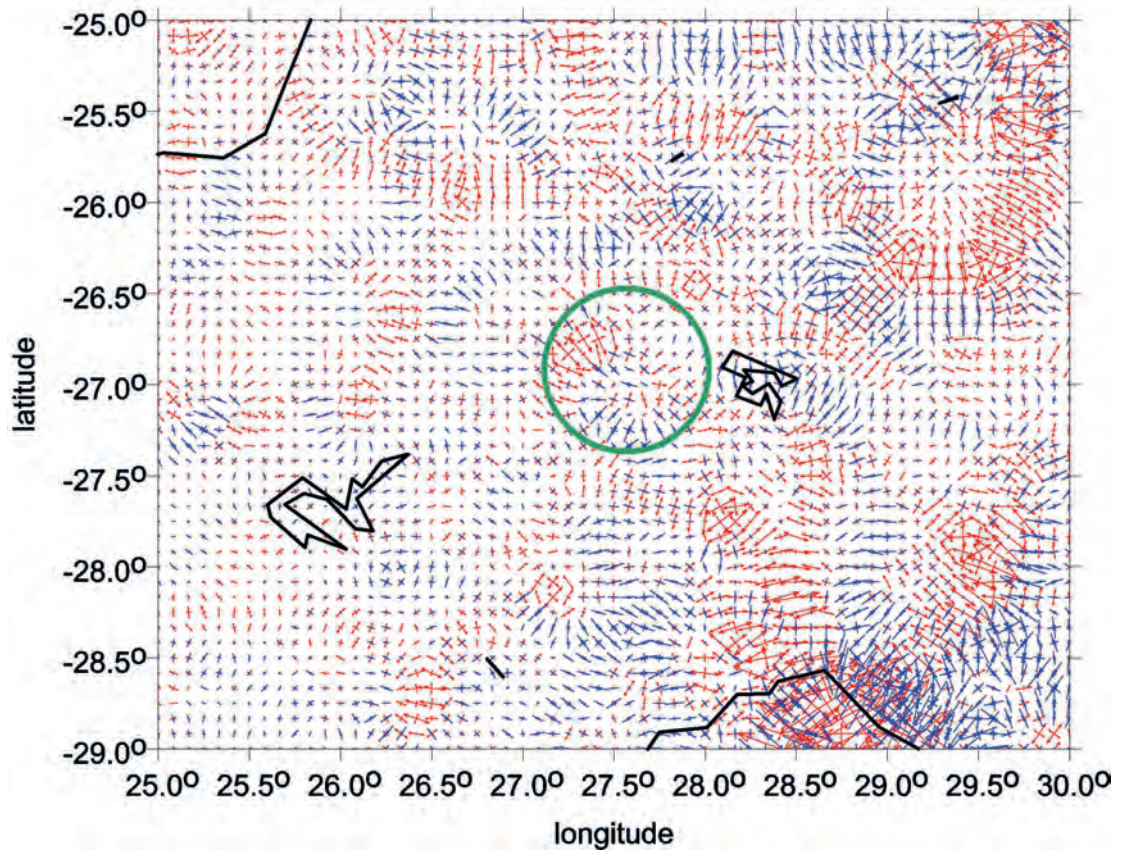**Fig. Vc** The strike angle θ_S for $I < 0.3$ (looking for flat objects).
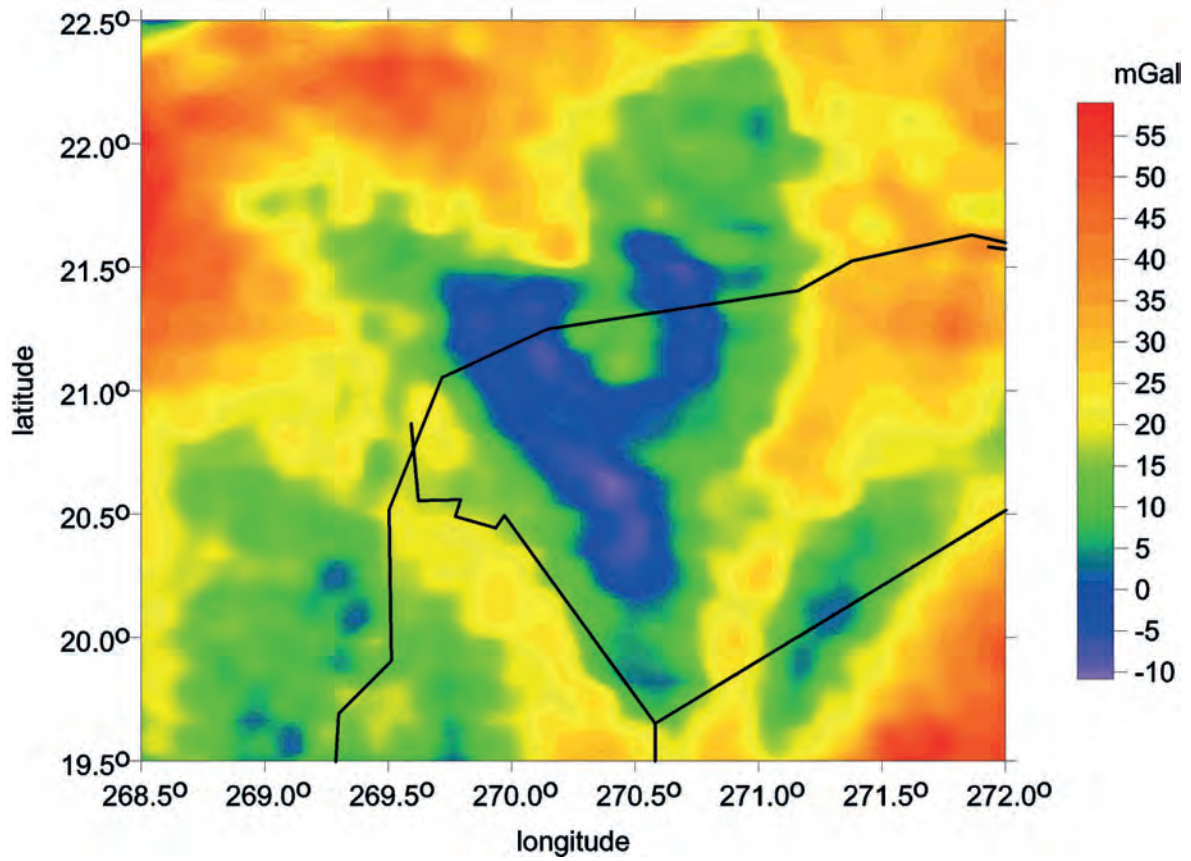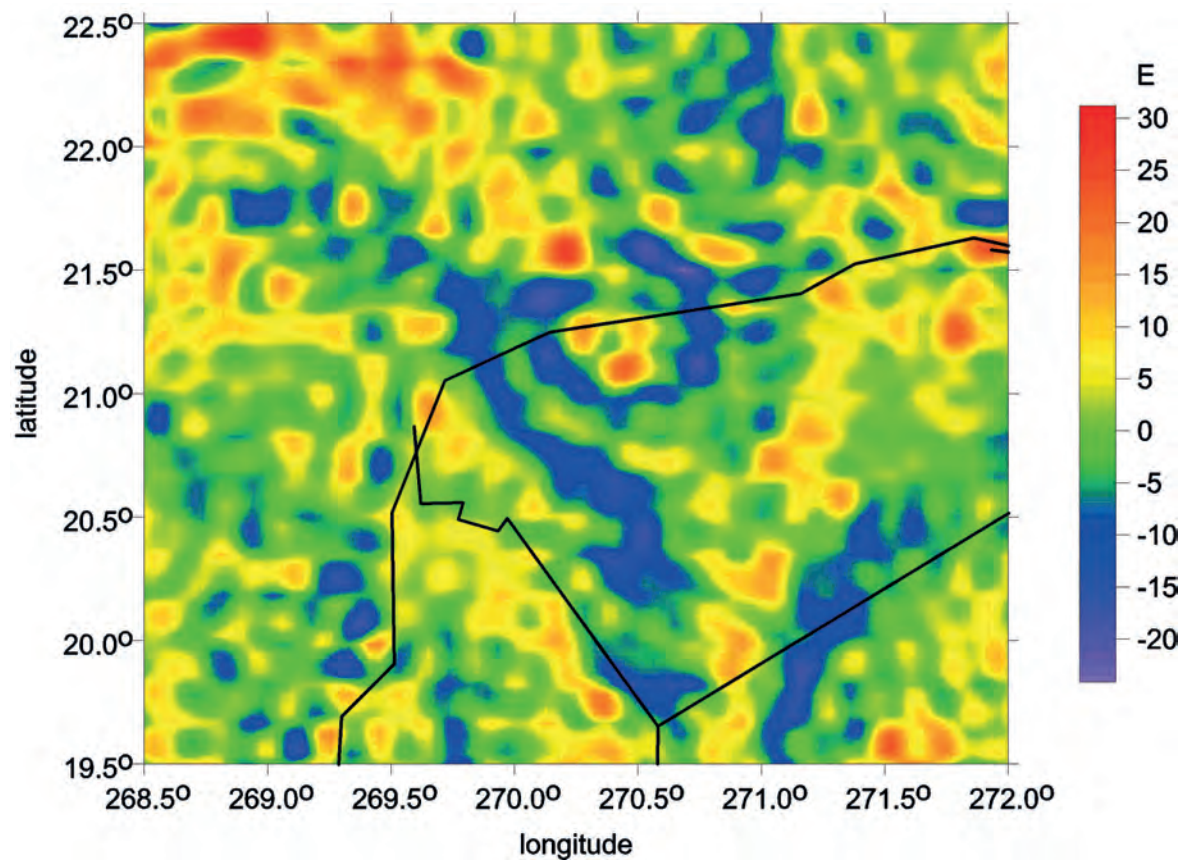

Fig. Vd The virtual deformations (red – dilatation, blue – compression) of the ellipse of deformation.

Fig. VI The Chicxulub impact crater, Yucatan.

Fig. VIa The gravity anomalies Δ*g*.

Fig. VIb The second derivative Γ_{33} of the disturbing gravitational potential.
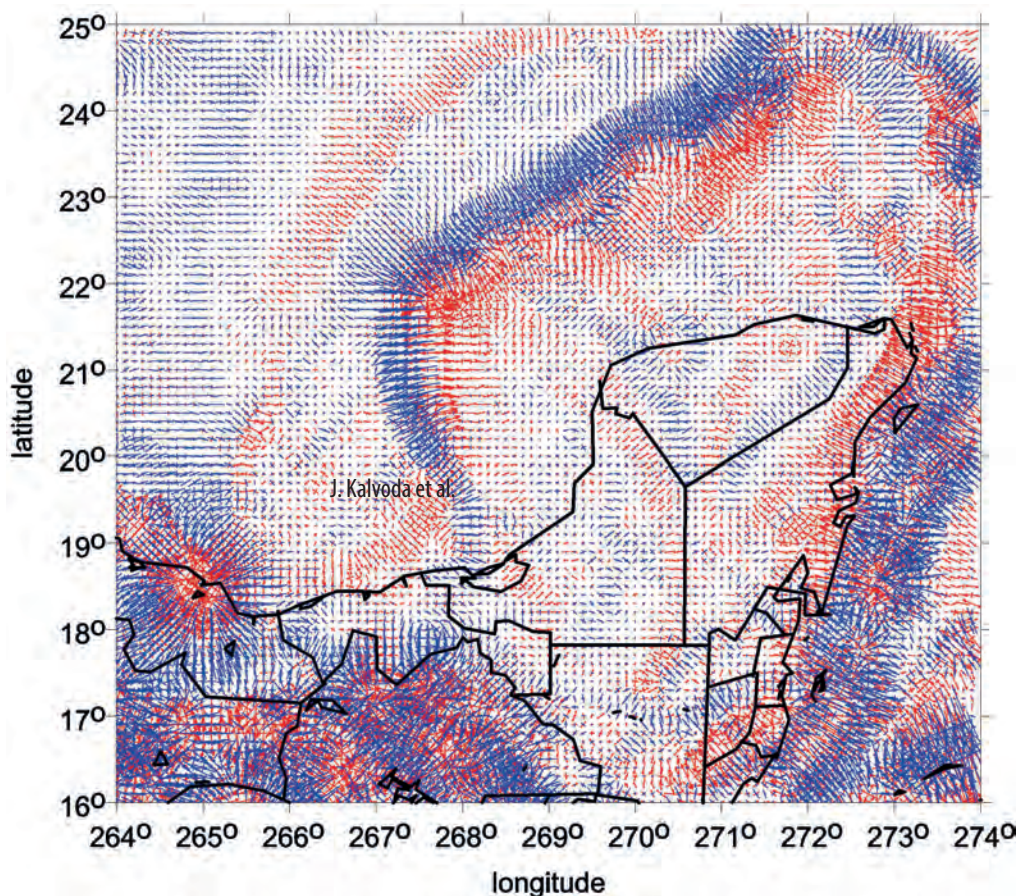
Fig. VIc The virtual deformations of the ellipse of deformation (red – dilatation, blue – compression) in the Mexico area and the Caribean (Campech bank).
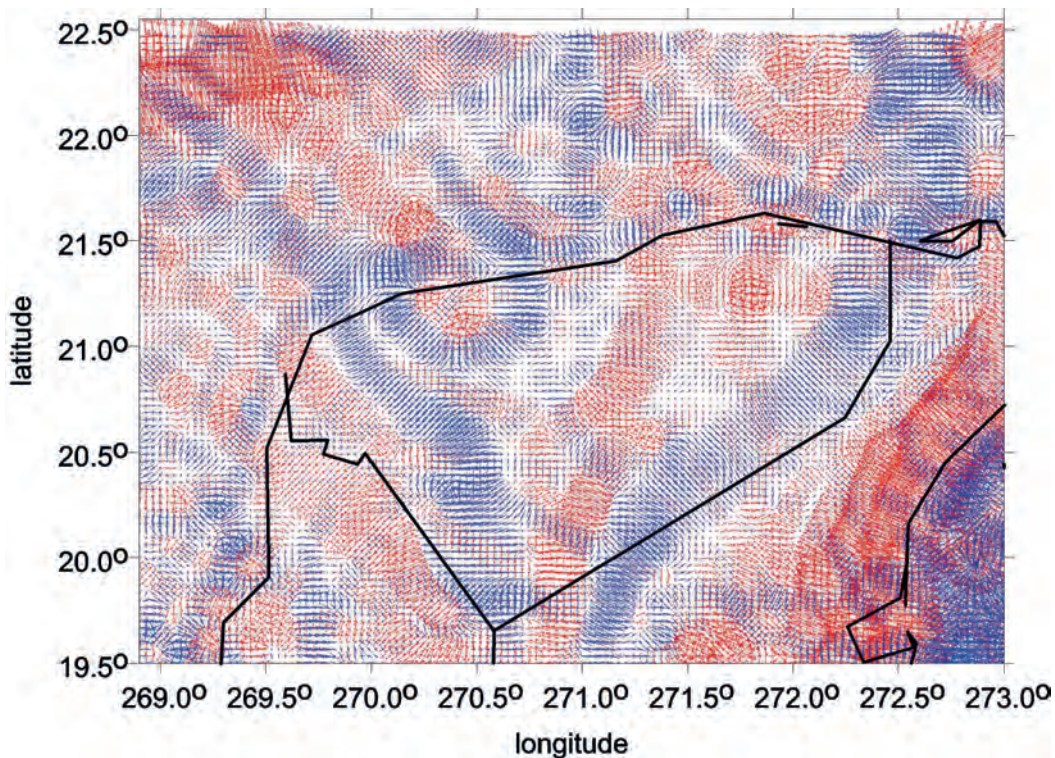

Fig. VId A detail of the round structure of the Chicxulub crater expressed by the virtual deformations of the ellipse of deformation (red – dilatation, blue – compression).
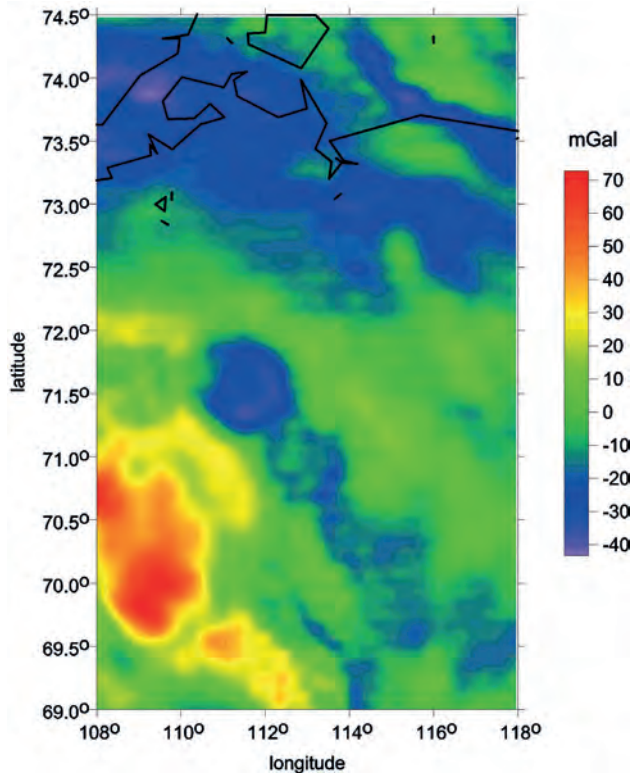
Fig. VII The Popigai impact crater, Siberia.

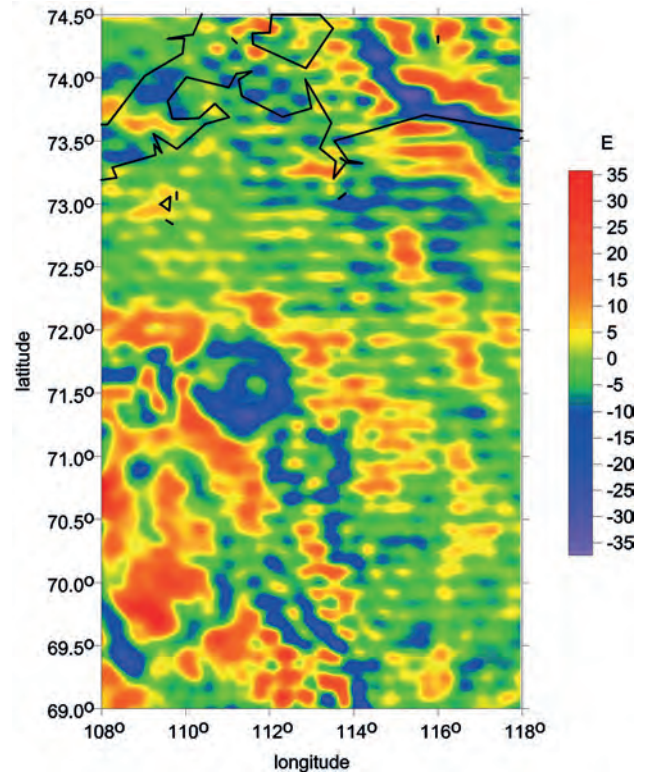
Fig. VIIa The gravity anomalies Δg.

Fig. VIIb The second derivative Γ_{33} of the disturbing gravitational potential.
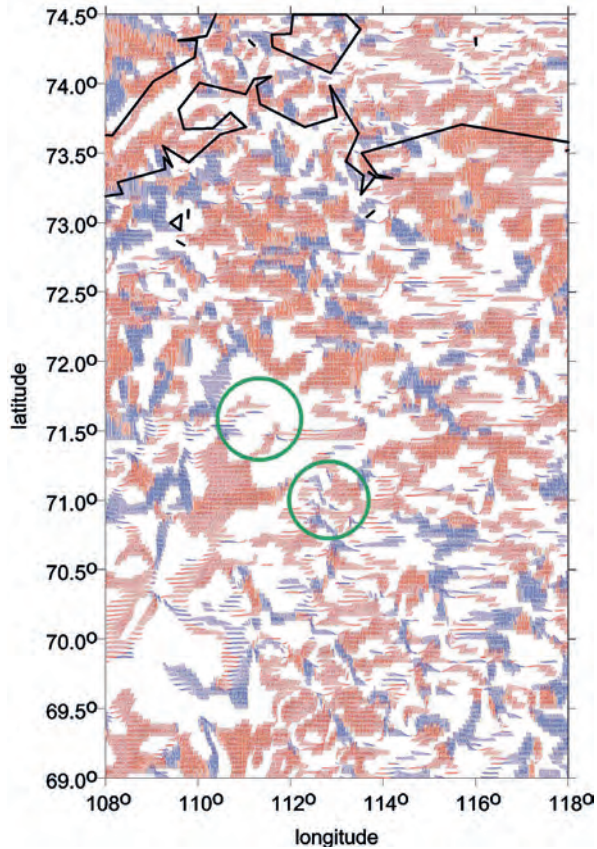
Fig. VIIc The strike angle θ_S for $I < 0.3$ (looking for flat objects).
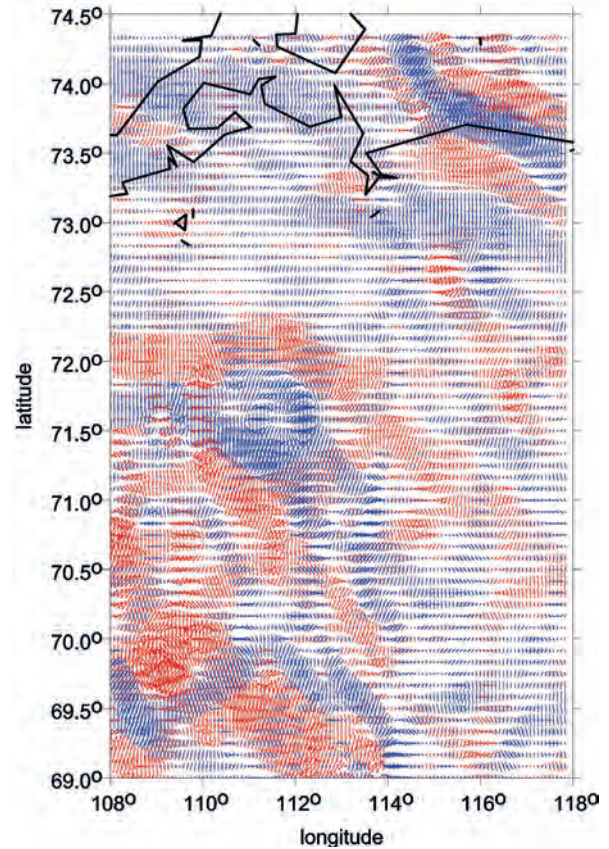

Fig. VIId The virtual deformations (red – dilatation, blue – compression) of the ellipse of deformation.

Fig. VIII The Lake Baikal region.

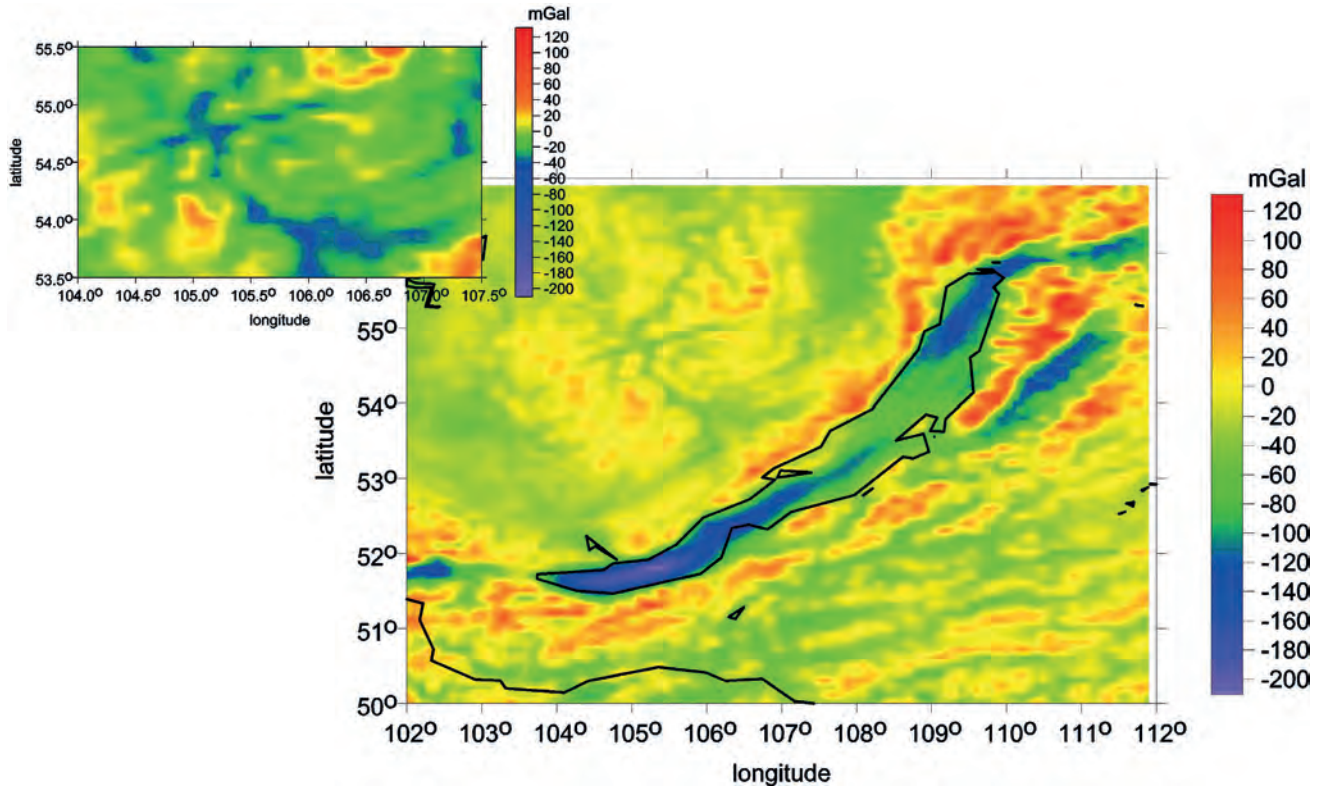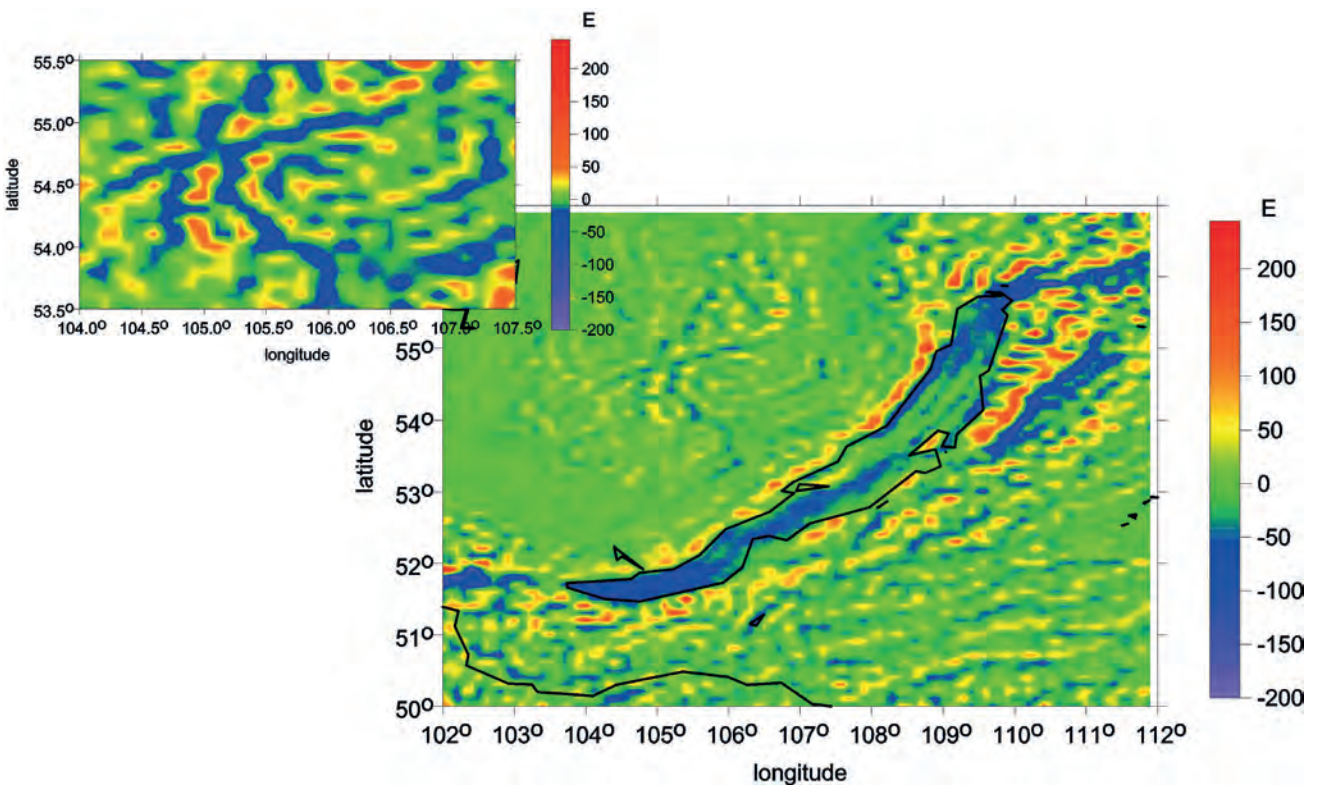**Fig. VIIIa** The gravity anomalies Δ*g*.

Fig. VIIIb The second derivative Γ₃₃ of the disturbing gravitational potential.

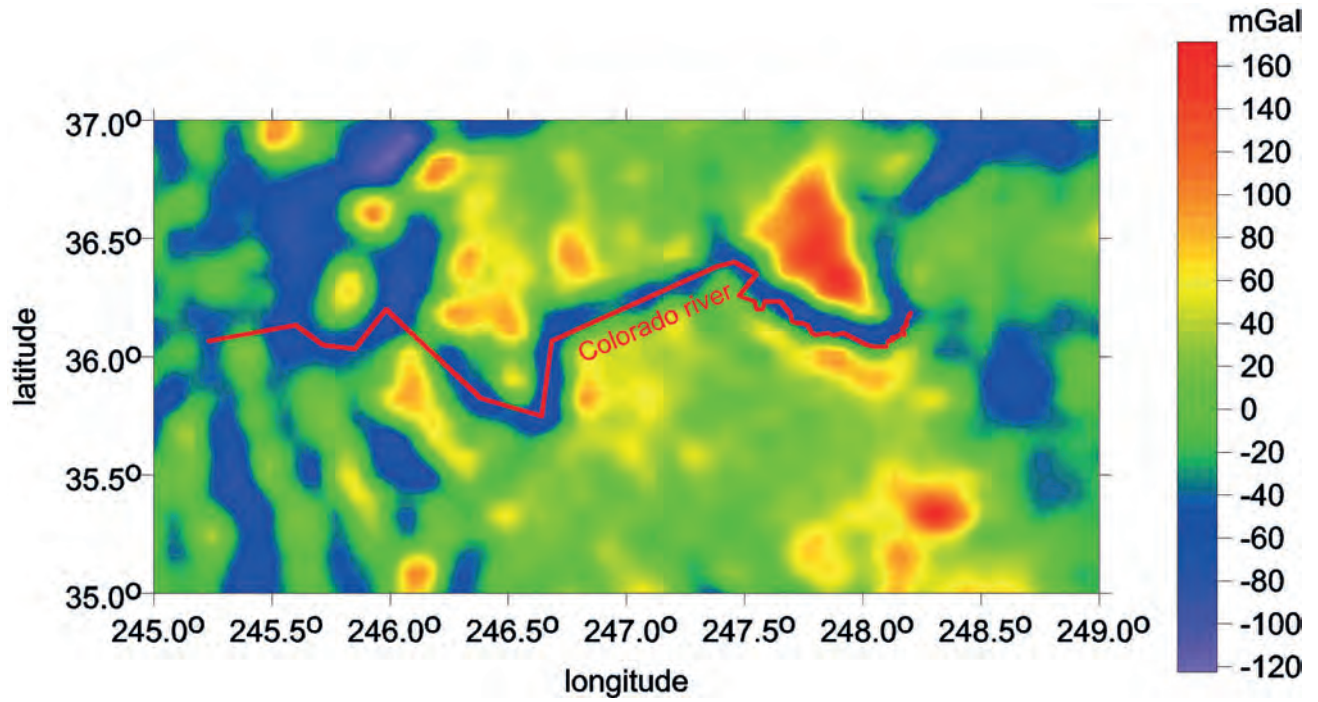**Fig. IX** The area of the Grand Canyon in Arizona. (Part of the Colorado River is shown by red lines).
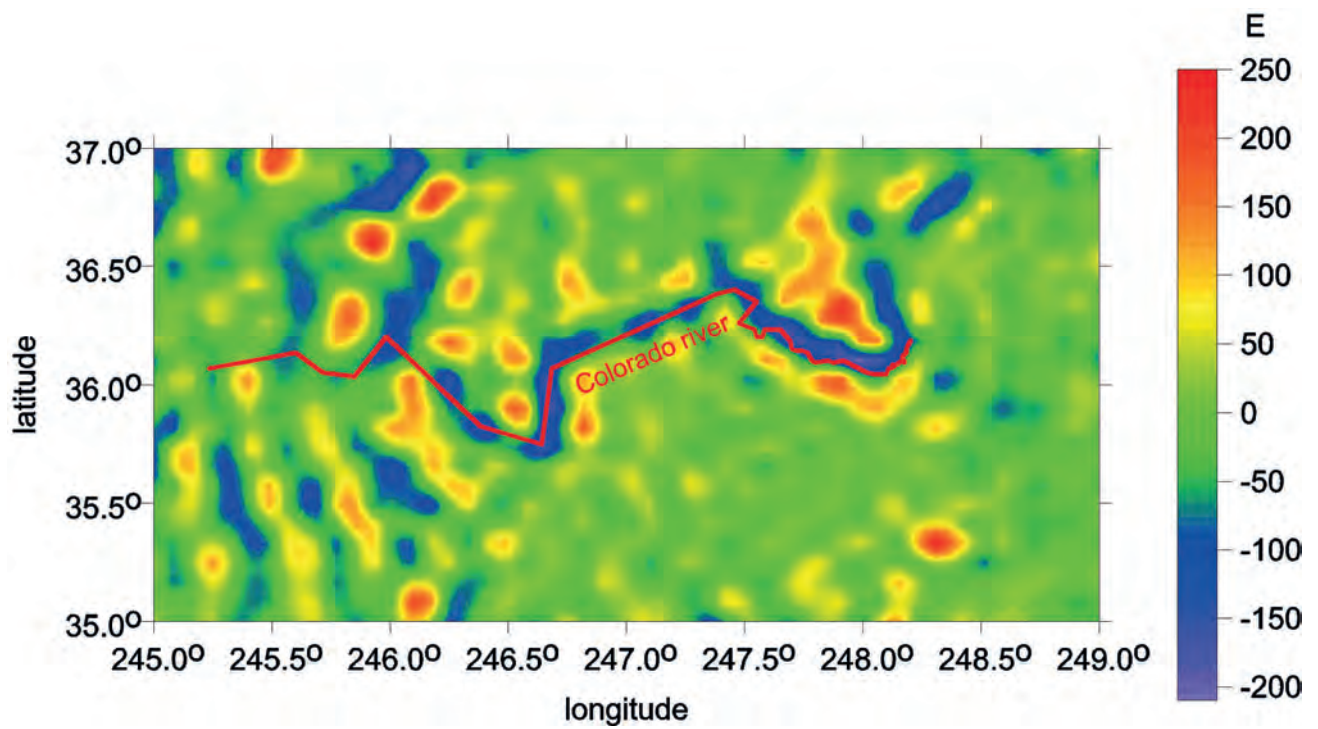

Fig. IXa The gravity anomalies Δ*g*.

Fig. IXb The second derivative Γ$_{33}$ of the disturbing gravitational potential.

Fig. X The area of the stratovolcanoes Popocatepetl (5426 m, P) and Iztaccihuatl (5230 m, I) in Mexico.
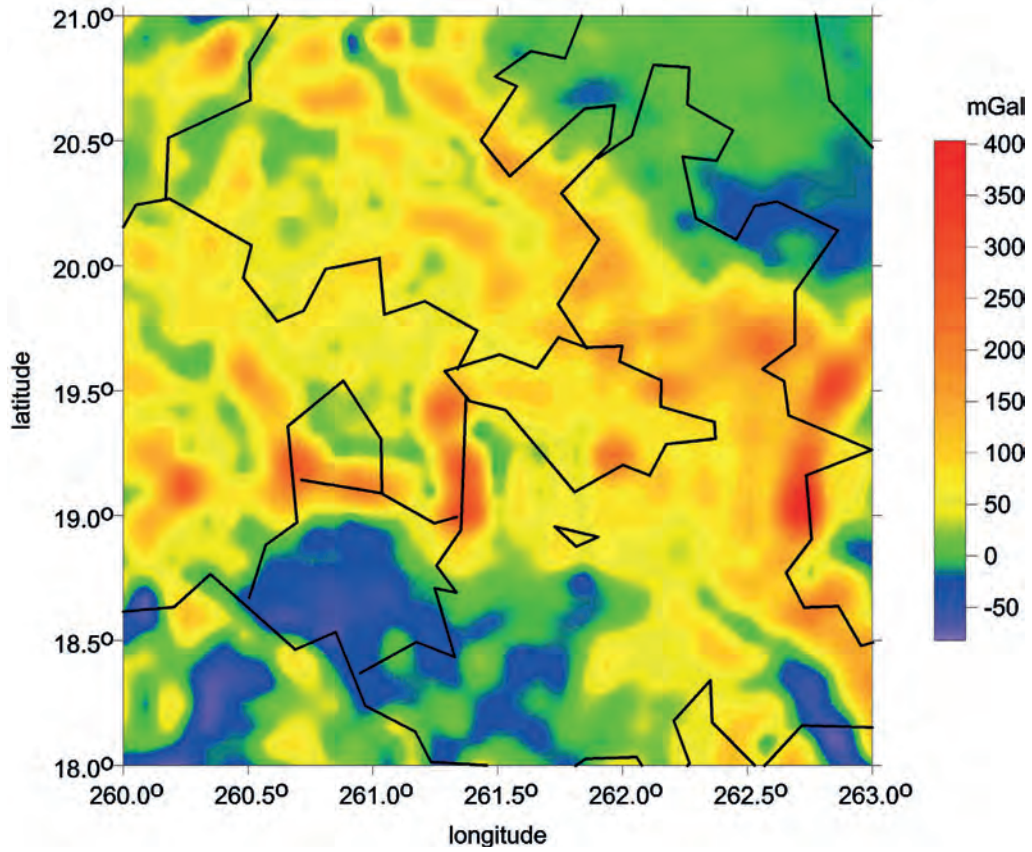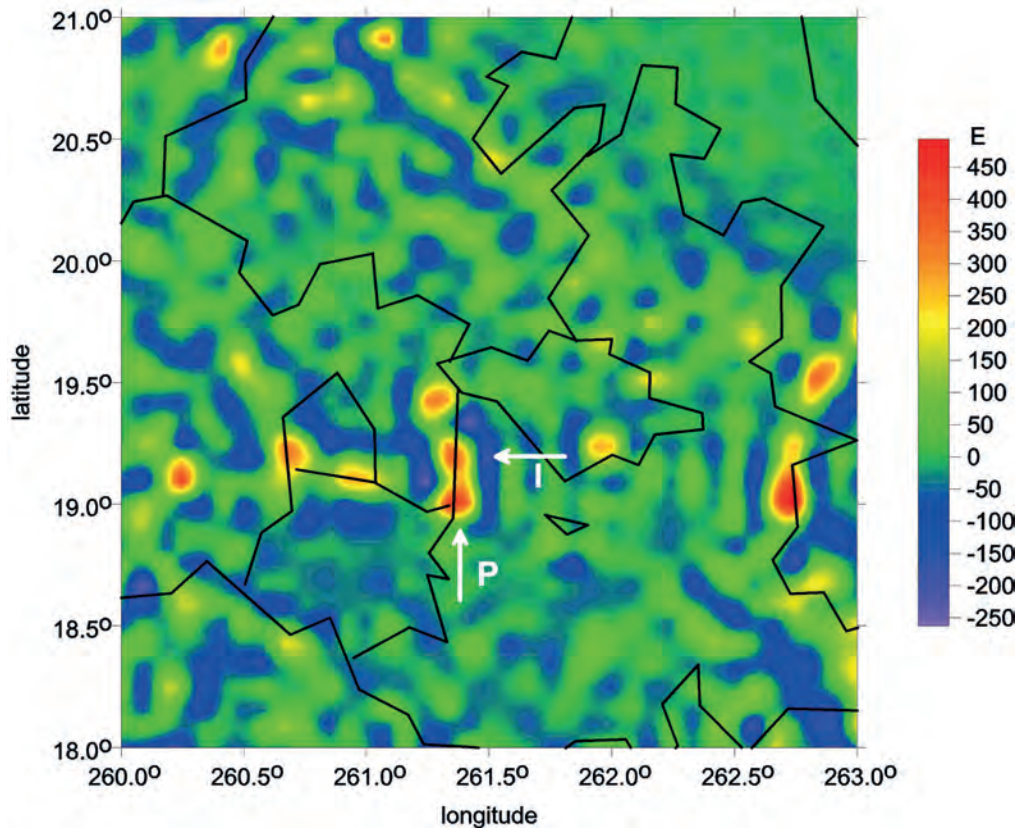

Fig. Xa The gravity anomalies Δg.

Fig. Xb The second derivative Γ_{33} of the disturbing gravitational potential.

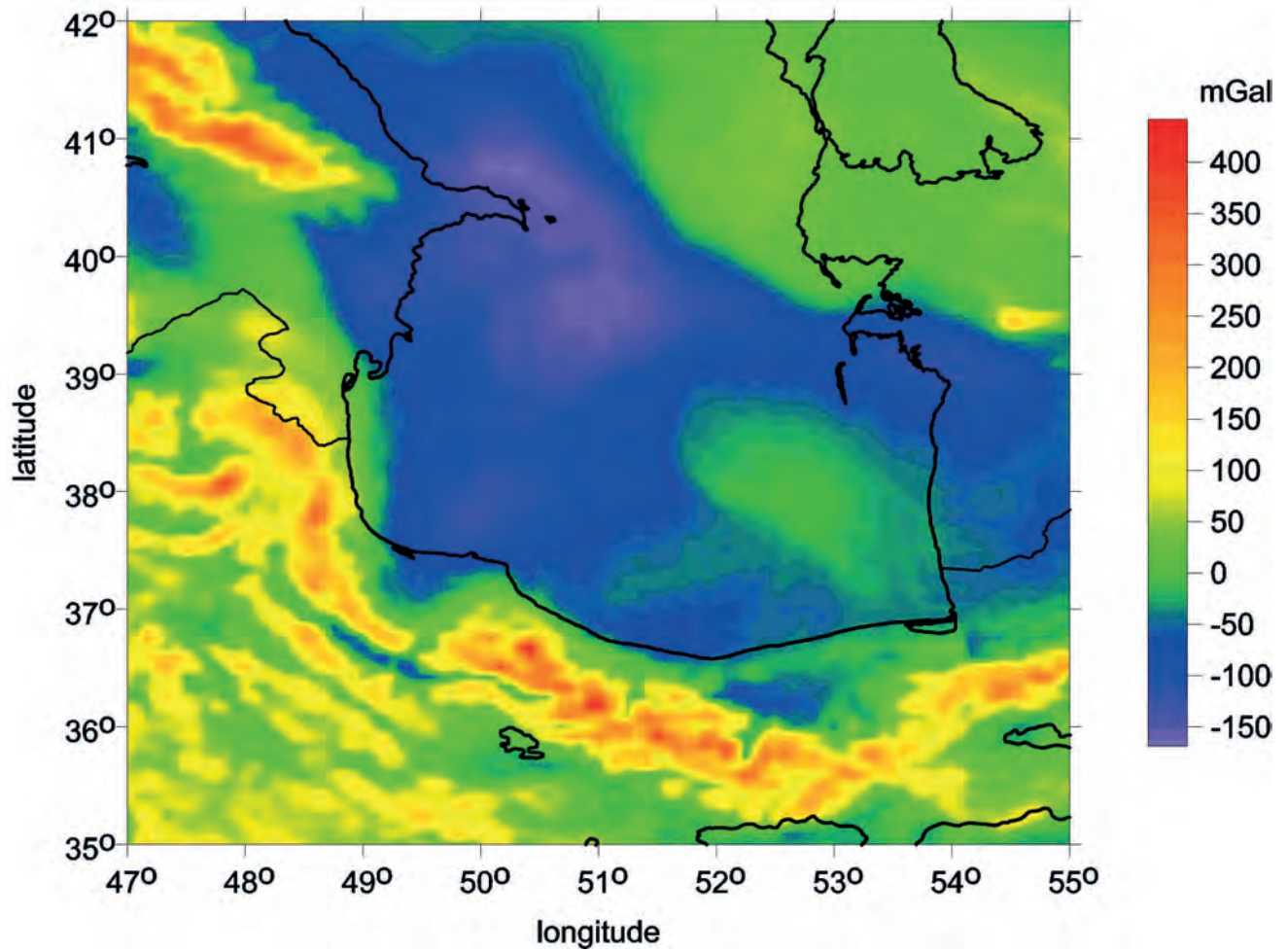**Fig. XI** Southern parts of the Caspian Sea and its neighbouring areas.
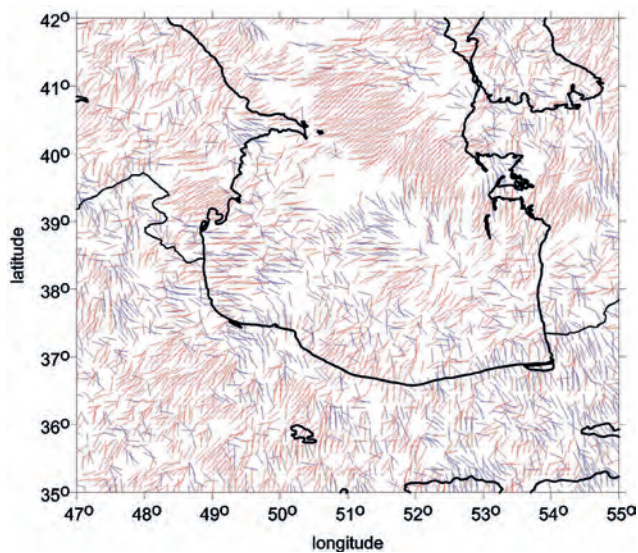

Fig. XIa The gravity anomalies Δ*g*.

Fig. XIb The strike angle θ_S for *I* < 0.3 (looking for flat objects). Note the belt of vectors oriented to one side crossing the central part of the Caspian Sea.
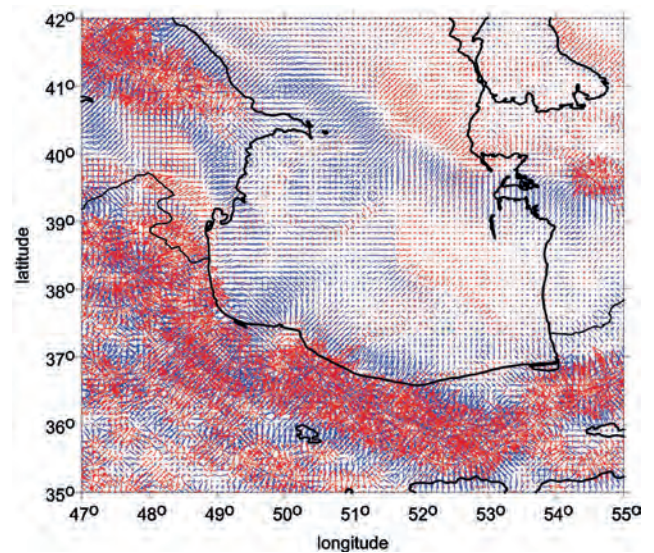
Fig. XIc The virtual deformations (red – dilatation, blue – compression) of the ellipse of deformation. A clear "belt" going roughly from West to East across the Caspian Sea.

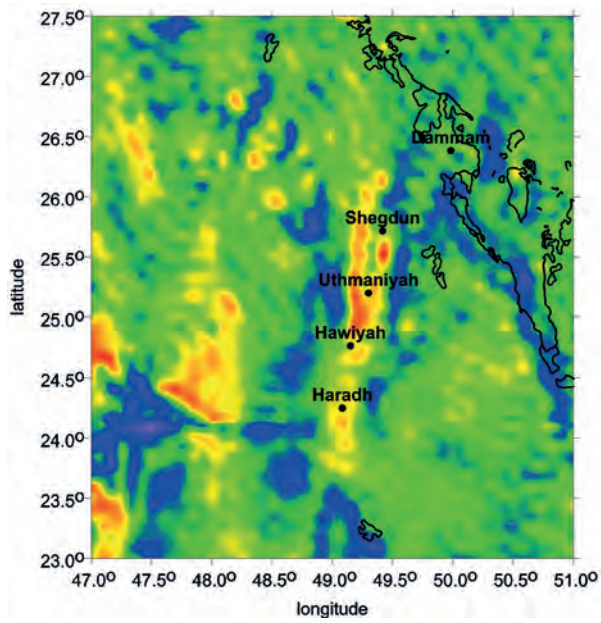**Fig. XII** The area of the Ghawar oil fields, Saudi Arabia.

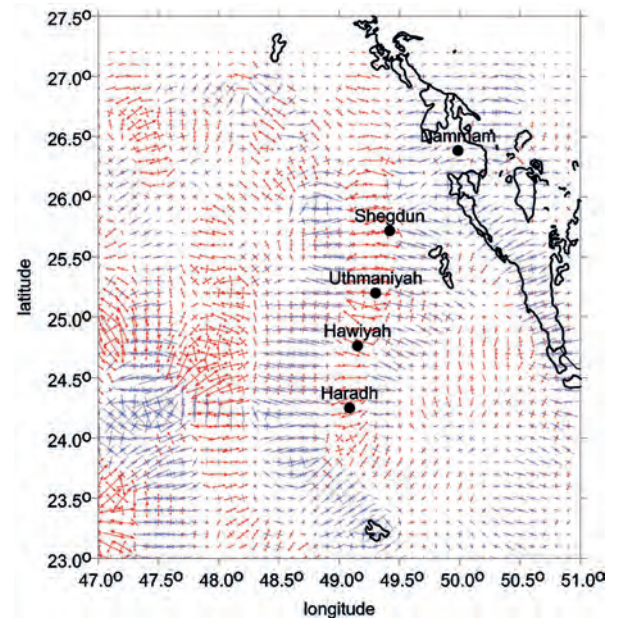**Fig. XIIa** The second derivative Γ_{33} of the disturbing gravitational potential.

Fig. XIIb The virtual deformations (red – dilatation, blue – compression) of the ellipse of deformation.
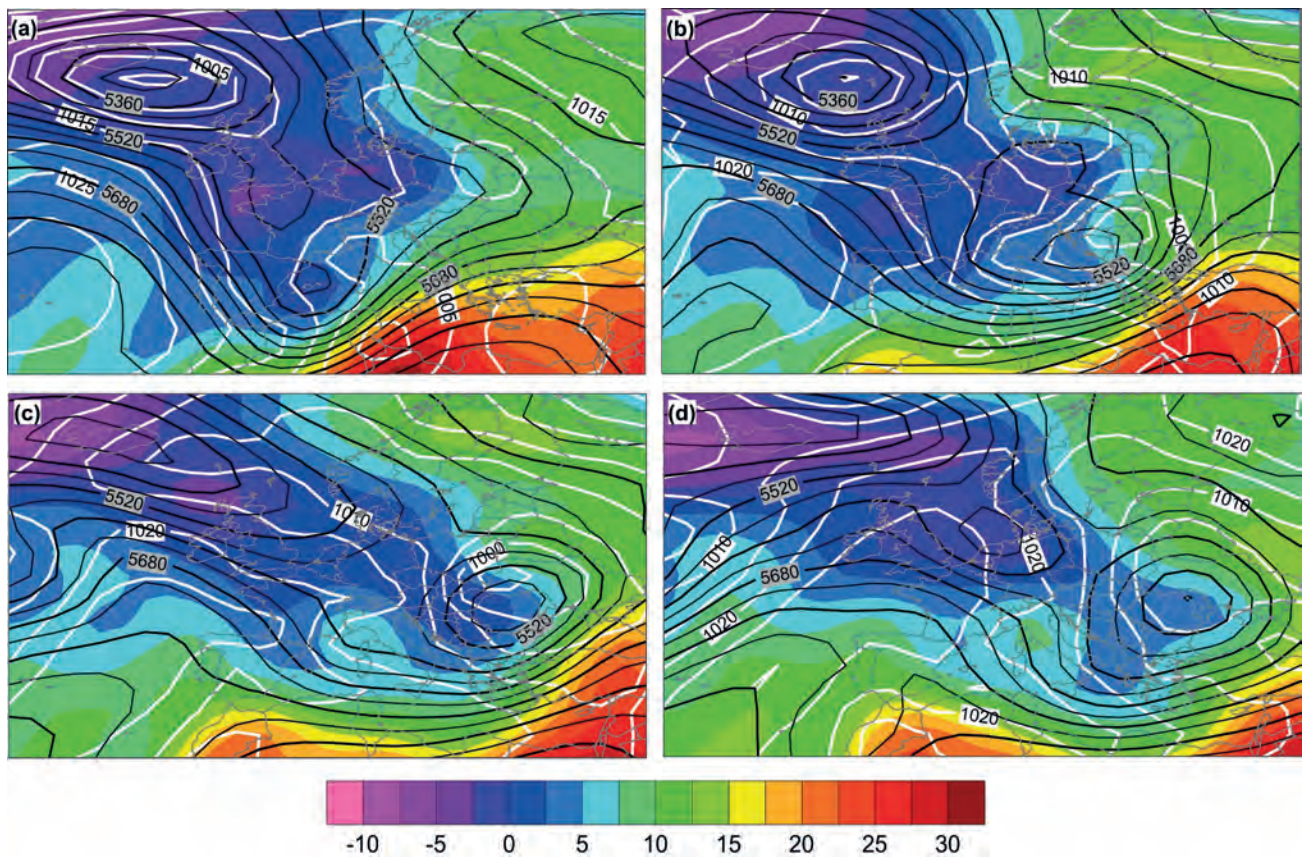

Fig. XIII NCEP-NCAR re-analyses of temperature [°C] at 850 hPa, geopotential height [m] of 500 level and sea level pressure [hPa] in Euro-Atlantic region just before and during the May 2010 event: (a) 14 May 2010 at 18 UTC, (b) 15 May 2010 at 18 UTC, (c) 16 May 2010 at 18 UTC, and (d) 17 May 2010 at 18 UTC.